Types of severe convective wind events in eastern Australia

Andrew Brown,[a,c] Andrew Dowdy,[b,c] Todd P. Lane,[a,c] Stacey Hitchcock,[a,c]

[a] *ARC Centre of Excellence for Climate Extremes, The University of Melbourne, Australia*

[b] *Australian Bureau of Meteorology, Melbourne, Australia*

[c] *School of Geography, Earth and Atmospheric Sciences, The University of Melbourne, Australia*

Corresponding author: Andrew Brown, andrewb1@student.unimelb.edu.au

ABSTRACT: Severe winds associated with thunderstorms and convection are a hazard affecting key aspects of society, including emergency management and infrastructure design. Several studies around the world have shown that severe convective winds (SCWs) can occur due to several different processes, in a range of atmospheric environments, with significant regional and temporal variations. However, in eastern Australia, the types of SCWs and their variability have not been assessed outside of individual case studies. Here, a combination of reanalysis, lightning, radar and station data are used to characterise a set of 36 SCW events in four locations in eastern Australia. These events are objectively chosen based on the strongest measured wind gusts from station data (greater than 25 m/s) over a 14-year period, with 6-hourly lightning data and a 30 dBZ radar reflectivity threshold used to infer moist convective processes. Radar data analysis suggests that these SCW events are produced by several different types of parent thunderstorms, with station observations suggesting a range of temporal characteristics for these different event types. A clustering algorithm applied to environmental data is used to suggest three dominant types of events, based on low-level moisture, low-level temperature lapse rate, and deep-layer mean wind speed and vertical shear. Based on the distribution of synoptic conditions and thunderstorm properties for each environmental cluster, it is suggested that these three event types correspond to: 1) shallow vertical transport of strong synoptic-scale winds to the surface, 2) downbursts driven by sub-cloud evaporation, and 3) intense thunderstorms including supercells.

SIGNIFICANCE STATEMENT: The purpose of this study is to better understand the different types of severe wind events in eastern Australia that are produced by convective storms. We looked at 36 historical cases in four locations and find that severe winds can be produced by very different classes of convective storms. We also suggest that there are three key types of atmospheric environment that are associated with events in this region. These environments vary in terms of the vertical structure of temperature, moisture, and wind speed above the surface. Understanding the different types of environments that lead to severe convective winds can help to reduce uncertainties in future climate projections for this region based on environmental changes.

1. Introduction

Severe winds associated with convective processes, including thunderstorms, are a significant hazard that can affect key sectors of society. In eastern Australia, wind gusts at a height of 10 m with an average recurrence interval longer than 20 years are produced mainly by convective processes (Holmes 2002), and are therefore an important factor to consider for infrastructure design and planning, while also posing a unique hazard to aviation and emergency management, for example (Potts 2002; Potter and Hernandez 2017; Oliver et al. 2000). As the physical processes and statistical properties of severe convective winds (SCWs) are distinct from severe synoptic-scale wind processes, they are often classified and analysed separately (Holmes 2002; Spassiani and Mason 2021), noting that SCWs may be embedded within large-scale weather systems such as cyclones and fronts (De Gaetano et al. 2014; Ludwig et al. 2015).

Previous studies have indicated that SCWs can occur due to a number of different physical mechanisms, within a range of atmospheric environments (Wakimoto 2001). Downburst wind events are driven by evaporation and sublimation of precipitation within the descending air of a thunderstorm cell, which may be initiated and/or sustained by the contribution of hydrometeor loading to negative buoyancy, with small-scale downbursts (less than 4 km across) known as microbursts (Wakimoto 1985; Atkins and Wakimoto 1991). Dry microbursts, with little or no precipitation at the surface, tend to occur in environments with a large amount of moisture available at the cloud base, and a relatively dry, warm sub-cloud layer, leading to the potential for enhanced evaporation and descending air with strongly negative buoyancy (Srivastava 1985; Proctor 1989). Wet microbursts, accompanied by precipitation at the surface, can occur due to similar processes, but in environments with high amounts of surface moisture and relatively low cloud bases, meaning that hydrometeor loading plays a large role in wet microburst production compared with dry microbursts (Atkins and Wakimoto 1991). Downbursts and microbursts can also exist within the rear flank of supercell thunderstorms in highly sheared, unstable environments, noting that severe surface winds can also be generated by pressure perturbations in these systems (Markowski 2002). Within mesoscale convective systems (MCS), which generally form in environments with significant vertical wind shear for storm organisation (Schumacher and Rasmussen 2020), large regions of evaporating precipitation can lead to strong downdrafts and outflow along the leading edge of the system, often causing widespread severe winds (Johns and Hirt 1987). The tilting of

these downdrafts due to vertical wind shear in some cases can lead to mesovortices within these systems (Weisman and Trapp 2003), which can also contribute to severe wind damage (Wakimoto et al. 2006). In addition, linear MCS can have mid-level rear inflow jets, which can lead to bow echo systems, while descending jets can lead to strong winds at the surface (Weisman 1992). Severe surface winds may also be generated by convective transport or vertical mixing of strong winds from above the surface, including within marginally unstable environments (Geerts 2001; Mahoney et al. 2009; Sherburn et al. 2021), often embedded in extratropical cyclones and their associated fronts (Ludwig et al. 2015; Pantillon et al. 2020). These types of events may be associated with relatively shallow convective storms, as investigated by Clark (2013) for "convective lines" in the United Kingdom.

These findings have led to several studies that have investigated the climatological occurrence frequency of various types of SCW events. For example, in some regions of the United States and Europe, SCWs are found to be most commonly produced by linear MCS (Gatzen 2013; Klimowski et al. 2003), while in other regions the distribution of storm types is shifted towards disorganised or cellular convection (Smith et al. 2013; Yang et al. 2017). The type of storms that typically produce SCWs may also depend on the time of year, as suggested by Pacey et al. (2021) who found that the majority of European cases in warm-season environments are produced by cellular convection, while events in cool-season environments tend to be associated with linear systems. Earl et al. (2017) constructed a climatology of extreme wind gusts from extratropical cyclones in the United Kingdom, and found that the strongest events tend to be associated with mesoscale convective features, such as sting jets and convective lines. In the southeastern United States, SCWs are often found to be produced by short-lived, "pulse" thunderstorms, with weak synoptic-scale forcing (Miller and Mote 2018). In sub-tropical eastern Australia, Geerts (2001) hypothesised that differences in the diurnal frequency distribution of SCW occurrences between inland and coastal locations are related to the type of parent thunderstorm, however "no direct information (was) available to classify the thunderstorms" in that study. Other studies in Australia have demonstrated the occurrence of several types of SCW events on an individual case basis, including Richter et al. (2014) who present an evaluation of a supercell storm with damaging gusts in the east Australian city of Brisbane, while Earl and Simmonds (2018) have described a case of linear convective wind storms driven by an extratropical cyclone in southern Australia. Although developments have been

made in understanding the climatological distribution of thunderstorm types in some regions of Australia (Potts et al. 2000; May and Ballinger 2007; Warren et al. 2020; Hitchcock et al. 2021), as well as the different types of large-scale environments for other hazards such as extreme rainfall (Warren et al. 2021), the distribution of SCW event types in Australia has not been systematically evaluated. This is in part due to limitations in the observational wind record and the small scale nature of SCWs, as well as difficulties in their classification as distinct from other non-convective wind events. The identification of different types of SCW events could help to reduce uncertainties in future projections based on changes to convective ingredients in Australia (Brown and Dowdy 2021b), noting that there has been limited amounts of research related to future projections of SCWs in other regions around the world (Seneviratne et al. 2021).

Here, a set of 36 SCW occurrences are examined from four locations in eastern Australia, in order to investigate the different types of events in this region. These SCW occurrences were defined by a previous study using daily maximum wind gust observations and 6-hourly lightning data (Brown and Dowdy 2021a). Each event is characterised based on the convective environment and synoptic features from ERA5 reanalysis data (Hersbach et al. 2020), the type of parent thunderstorm based on radar-derived storm statistics, lightning observations, and weather station observations at one-minute frequency. High-resolution observations from radar, lightning and weather station networks are intended to provide details on the mesoscale features associated with these events, building on the original analysis of Brown and Dowdy (2021a). To provide some additional context around the convective environment and synoptic features for the SCW events, these conditions are also compared with their climatological occurrences at each location based on probability distributions calculated over a 14-year period. In addition, the events are sorted into clusters based on their convective environment, allowing for an assessment of possible event types. This assessment also includes considering composite vertical soundings for each cluster, providing additional details for helping aid the interpretation of physical processes associated with each cluster.

The remainder of this paper is structured as follows: In Section 2, the case selection process is outlined, as well as the observational datasets and methods used to characterise each SCW event. In Section 3 details of each event are presented, which are then used to suggest a classification of event types for this region based on statistical clustering. In Section 4, a discussion of the results is presented, prior to some concluding comments and a summary of the findings in Section 5.

2. Data and methods

a. Severe convective wind dataset and event locations

In this study, cases are selected based on SCW events identified previously for Australia by Brown and Dowdy (2021a), over a 14-year period from 2005 to 2018. Here, the Brown and Dowdy (2021a) dataset is described, and four locations in eastern Australia are chosen for further analysis. The method of selecting cases from this dataset at these locations will be described further in Section 2c.

Events are defined by Brown and Dowdy (2021a) using daily maximum wind gust observations from Automatic Weather Stations (AWS) greater than 25 m/s (3-second average wind speed at 10 m above ground level), which occur in the presence of lightning. The threshold of 25 m/s is consistent with the criteria for damaging winds in Australia used by the Bureau of Meteorology. Lightning data were used by Brown and Dowdy (2021a) to associate a severe wind gust with convective processes in line with previous studies in other regions (Mohr et al. 2017; Yang et al. 2017; Smith et al. 2013). Lightning strokes for each gust event were obtained from two data products combined on a 0.25-degree spatial grid: the World-Wide Lightning Location Network (WWLLN, Virts et al. (2013)), and the Global Position and Tracking System (GPATS). In their study, a wind gust measured at an AWS was considered convective if any grid box within 50 km had at least two observed lightning strokes within the closest 6-hourly period.

For the current study, cases will be selected from four eastern Australian locations within the dataset of Brown and Dowdy (2021a). Event locations are shown in Figure 1 and include three extratropical coastal locations at different latitudes (Melbourne, Sydney and Brisbane), and an inland location in southern Australia (Woomera). These locations are chosen based on having a sufficient number of SCW events (see Section 2c), sampling climatic variability (see National Resource Management regions in Figure 1), retaining proximity to high-quality weather radar with archived data, and being within regions where SCWs are important for the extreme wind climate (Holmes 2002). Brown and Dowdy (2021a) use one AWS to detect SCWs in the Melbourne (Melbourne Airport), Sydney (Sydney Airport), and Woomera (Woomera Aerodrome) locations, while for Brisbane, both the Amberley AWS and Oakey Aerodrome are used (Figure 1).

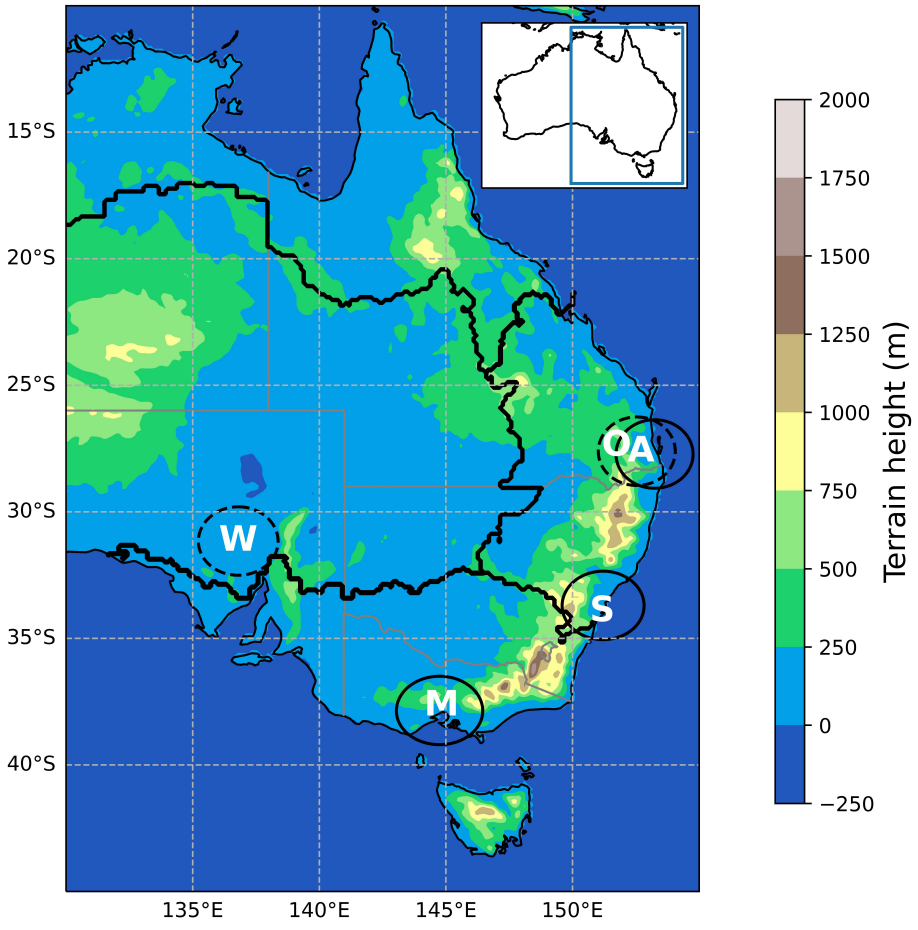

FIG. 1. The locations of AWS used to define SCW cases from Brown and Dowdy (2021a), including for Melbourne (M), Sydney (S), Brisbane (Oakey marked with an "O", Amberley marked with an "A"), and Woomera (W). For each AWS, the range of the closest radar (150 km) is indicated by either a black solid circle (if the radar has archived Doppler wind measurements) or a dashed circle (without Doppler wind measurements). Topography data, provided as part of the Bureau Atmospheric Regional Reanalysis for Australia at 12 km spatial resolution (BARRA; Su et al. (2018)) is contoured. National Resource Management (NRM) super-cluster regions, which are often used to distinguish broad areas of similar climatic conditions (CSIRO and Bureau of Meteorology 2015), are shown by black lines in the interior of the continent, and includes Eastern Australia (containing Sydney and Brisbane), Rangelands (containing Woomera), and Southern Australia (containing Melbourne).

b. Radar data and storm properties

For each potential SCW case in the Brown and Dowdy (2021b) dataset at the locations in Figure 1, parent storms are identified in this study using radar reflectivity data obtained from the

Australian Unified Radar Archive (AURA; Soderholm et al. (2019)), on a grid with 1 km horizontal and 500 m vertical spacing. The radars used here are Melbourne (for Melbourne Airport AWS), Terrey Hills (for Sydney Airport AWS), Mt. Stapylton (for Amberley AWS), Marburg (for Oakey Aerodrome AWS), and Woomera (for Woomera Aerodrome AWS). For further analysis of each parent storm, AURA also contains a convective pixel classification that is determined using the method of Steiner et al. (1995). For certain radars, including Melbourne, Terrey Hills, and Mt. Stapylton, Doppler velocities are also available, as well as azimuthal shear that is computed from the gridded velocity data following the method of Miller et al. (2013). Azimuthal shear data will be used here to characterise storm rotation in line with previous studies (Smith et al. 2012). It is noted that Doppler velocities and azimuthal shear are not available for the the Woomera and Marburg radars. It follows that for potential events in the Brisbane domain, the Amberley AWS will be prioritised over the Oakey AWS (detailed further in Section 2c).

For identifying parent storms, the tobac python package (Heikenfeld et al. 2019) is first applied to smoothed 2-d fields of column-maximum reflectivity (either at 10-minute or 6-minute frequency depending on the radar). A reflectivity threshold of 30 dBZ was used in tobac to segment the smoothed reflectivity data into storm objects, with this threshold similar to other studies of convective systems in eastern Australia (Potts et al. 2000; Hitchcock et al. 2021). Objects also have minimum size, volume, and height requirements of 15 km^2, 30 km^3 and 2 km, respectively. The size threshold is based on a previous study for Australia (Soderholm et al. 2017), and is intended to allow for the identification of relatively small, cellular events, while ignoring radar artifacts that may only be a few pixels in size. A 2 km height limit is also intended to remove radar artifacts, namely ground clutter, while still retaining shallow convective storms. The storm object with the highest maximum reflectivity value, within 10 km at the most recent scan before each event, is assigned as the parent storm. The proximity threshold of 10 km is chosen to account for the propagation of convective outflow ahead of a storm, in line with previous studies (Lagerquist et al. 2017).

A modified version of the TINT python package (Raut et al. 2021) is then used to track segmented objects in time and to compute storm properties by fitting an ellipse to the object. The properties computed include the major axis length, aspect ratio, number of local reflectivity maxima within the object, the convective pixel fraction, and maximum object altitude. In addition, the 99.5th

percentile of azimuthal shear between 2 and 6 km altitude within the object will be used for an assessment of potential storm rotation. A temporal filter is applied to the 99.5th percentile of azimuthal shear, with the rolling hourly median used to ensure that any rotation is sufficiently long-lived. For all of the above-mentioned properties, values at the most recent scan before each SCW event will be reported. These storm properties will also be used to develop a method for objective storm classification, with the results of that development process described in Section 3a.

c. Case selection

In the current study, SCW events from Brown and Dowdy (2021a) at each of the four locations described in Section 2a (see Figure 1) are selected as cases for further analysis. This is done by choosing a set of the strongest measured gusts, with the constraint that these gusts have associated archived radar reflectivity data, and a storm object within 10 km for analysis (with storms identified following Section 2b). These radar constraints imposed on the original dataset of Brown and Dowdy (2021a) are necessary to analyse the parent storm associated with each potential SCW event. A total of 61 potential events were available from the Brown and Dowdy (2021a) dataset, including 11 for Melbourne, 13 for Sydney, 19 for Brisbane (including Oakey and Amberley), and 18 for Woomera (see Figure 2). Of these 61 events, seven were not suitable for selection due to not having a nearby storm object within 10 km, while four were not suitable based on having no associated radar reflectivity data. It is possible that the seven events that did not have a nearby storm object may not have been of a convective origin, although these events are not investigated any further here.

From these potential SCW events, the nine with the strongest gusts are selected at each location (with events that occur earliest selected for ties), meaning a total of 36 cases to be analysed further in this study. This number of 36 events (nine at each of the four locations) was chosen given that it is large enough to allow multiple instances of several event types to be considered, which could help reduce the risk of drawing conclusions based on anomalous single events, while still being small enough to allow for analysis on an individual event basis rather than relying only on summary statistics. The rank-gust distribution for the Brown and Dowdy (2021a) dataset is shown in Figure 2 for each AWS, including for the events that are selected for this study, and events that are discarded. Figures 2d and e show that for the Brisbane domain, the gust distribution for the Amberley AWS is

weaker than for Oakey AWS, although all four events from Amberley are selected here due to the availability of Doppler velocity data at that location (Section 2b), with the remaining five events for Brisbane selected from Oakey. Details of the selected set of 36 cases are presented in the results (see Table 1, for example).

d. High-resolution weather station observations and lightning data

To understand the evolution of each SCW event selected in Section 2c, two high-resolution observational datasets are used, including global lightning strokes aggregated at one-minute frequency, and station observations of rainfall and wind gust intensity measured at one-minute frequency (noting the gust data are a one-minute maximum of 3-second average wind speed). The high-resolution lightning data is complementary to the 6-hourly data used by Brown and Dowdy (2021a) to define their event dataset, and also uses WWLLN (Section 2a). For each SCW event, a time series of the number of lightning strokes in a 50 km radius around the event is analysed, and summarised by the total number of strokes over the hour centred on the peak gust.

The station observations are taken from the same set of AWS that measure the SCW events. The one-minute AWS rainfall data are presented as an accumulation over the span of each SCW event, defined as two hours before and after the event. The gust data is also presented for two hours either side of the event peak, and is used to calculate the peak-to-mean wind gust ratio for each event. The peak-to-mean wind gust ratio is defined here by dividing the peak event intensity by the mean wind gust over a four hour period, centered on the event, and has been used by previous studies to identify convective gust events (Durañona et al. 2007; Holmes et al. 2018).

e. Convective environment and clustering

To analyse the convective environment of each selected SCW event, diagnostics are computed from a combination of pressure-level and surface-level data from the ERA5 reanalysis (Hersbach et al. 2020), which is available on a global 0.25-degree horizontal grid. Specifically, we investigate four key diagnostics that we hypothesise to be relevant for thunderstorm occurrence, organisation, and severe surface wind potential. These include measures of low-level moisture (mass-weighted mean water-vapor mixing ratio from 0–1 km, Qmean01), low-level temperature lapse rate (from 1–3 km, LR13), deep-layer mass-weighted mean wind speed (from 0–6 km, Umean06), and deep-

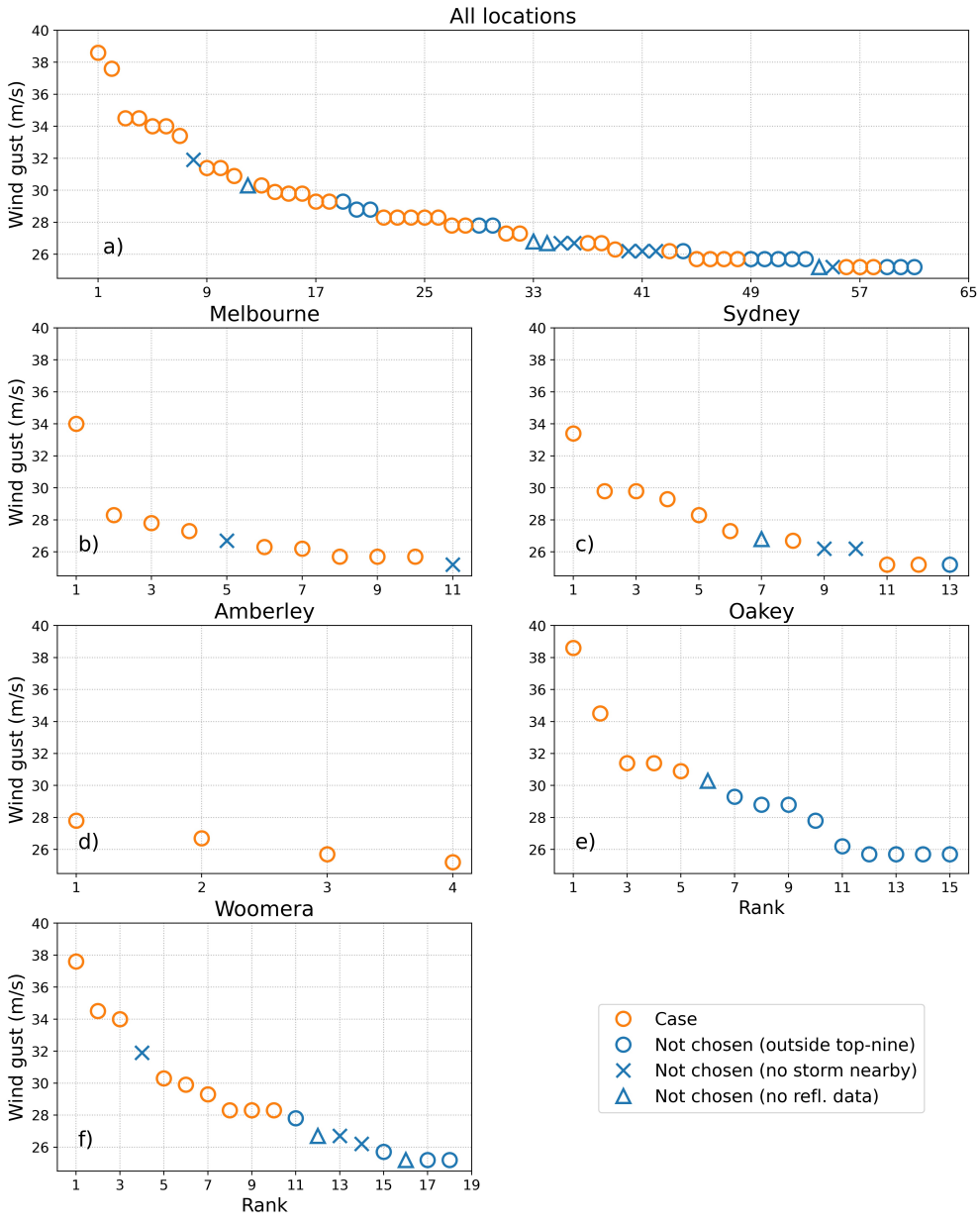

FIG. 2. a) Rank-gust distribution for all events in the Brown and Dowdy (2021a) dataset, for the four locations chosen for this study. This includes events measured at five AWS: (b) Melbourne, (c) Sydney, (d) Amberley, (e) Oakey, and (f) Woomera. Gusts that are selected as cases for this study are shown as orange circles, with all other gusts shown by blue markers. For gusts that are discarded, the markers shown are based on the reason why the gust was excluded: outside the top-nine strongest gusts (blue circles), no nearby storm object as inferred from radar data (blue crosses), or no associated radar data archived (blue triangles).

layer vertical wind shear (from 0–6 km, S06). These diagnostics have been been identified by previous studies to be relevant for SCWs in Australia (Brown and Dowdy 2019, 2021a), noting that low-level moisture is strongly related to convective available potential energy (CAPE) variability (Ye et al. 1998), while low-level lapse rates are related to downdraft potential by enhancing the negative buoyancy of descending air parcels (Srivastava 1985; Pryor 2015). However, downdraft potential also depends on the downdraft initiation conditions in the mid-troposphere and low-level humidity (Atkins and Wakimoto 1991). Deep-layer wind shear is related to convective organisation (Weisman and Klemp 1982), while strong deep-layer mean wind speeds represent strong winds aloft that can potentially be transported to the surface by convective processes and vertical mixing (Geerts 2001). Spatially, all four diagnostics (Qmean01, LR13, Umean06, and S06) are matched to a SCW event by using the maximum value over all ERA5 land grid points within 50 km of the AWS location, in order to account for errors in the timing and locations of air-mass boundaries within the reanalysis. Temporally, diagnostics are matched to a SCW event by using the most recent hourly time step before the event, with this method intended to represent pre-convective conditions.

Environmental conditions for the set of SCW events are compared to the climatological distribution using 6-hourly ERA5 data from 2005-2018 at each location, at 0000, 0600, 1200, and 1800 UTC. This analysis is performed separately using a convective and non-convective environmental climatology. The convective climatology is defined by 6-hourly lightning occurrences, and the non-convective climatology is defined by all 6-hourly time steps without lightning. Lightning occurrences used in the construction of the convective climatology are defined in the same way as for the Brown and Dowdy (2021a) SCW dataset described in Section 2a, by using data on a 0.25-degree grid from two lightning datasets (GPATS and WWLLN), and considering two or more strokes within each 6-hourly period centered on the ERA5 data. The convective climatology is referred to as an "ordinary" convective climatology, given that it does not include the SCW events examined here.

K-means clustering is used to identify dominant convective environment types, following several studies such as Pacey et al. (2021) for SCWs in Europe and Warren et al. (2021) for extreme rainfall in Australia, noting that other clustering methods have also been applied for some studies (for example, Zhou et al. (2021) for global hail environments using self organising maps). The choice for the number of clusters will be based on the silhouette score, which is described in the

Appendix, as well as the consistency of clustering based on data from ERA5 and data from a separate reanalysis, the Bureau Atmospheric Regional Reanalysis for Australia (BARRA; Su et al. (2018)). A second reanalysis is used in order to consider the stability of the clustering method to changes in the input, noting that the representation of SCW environments and synoptic conditions between ERA5 and BARRA are qualitatively similar for the events in this study (not shown), such that only ERA5 is used for the remainder of the analysis. The consistency between ERA5 and BARRA clusters will be assessed quantitatively by the Rand score, described in the Appendix, as well as qualitatively by comparing the environmental and storm characteristics of each cluster between reanalyses. It is noted that the addition of other commonly used convective diagnostics, such as storm relative helicity, CAPE, and downdraft CAPE, did not change the nature of the clusters presented in Section 3d based on the four diagnostics discussed above (Qmean01, LR13, Umean06, and S06), providing confidence that these diagnostics explain a significant amount of the variability in SCW environment types across these locations.

f. Synoptic analysis

Complementary to convective environment analysis, synoptic-scale features associated with each SCW event are analysed by computing diagnostics including the gradient in wetbulb potential temperature on the 700 hPa surface (GradT700), and geostrophic vorticity on the 500 hPa surface (GV500) from ERA5 data. This follows the method of Dowdy and Catto (2017) for the identification of conditions associated with synoptic-scale frontal systems (GradT700) and cyclones (GV500), including those which are collocated with favourable convective environments.

A single value of GradT700 and GV500 are associated with each SCW event, by taking maximum (for GradT700) and minimum (for GV500) values within a 500 km radius around the location of the AWS that measured the event. There is no clear optimal distance for associating synoptic-scale features with individual weather events, and here 500 km is chosen based on previous studies (Dowdy and Catto 2017; Pepler et al. 2021), and by visually inspecting the distance between fronts/cyclones and SCW events for individual cases (maps for each case are provided in the Supplementary Material). Although values of GV500 and GradT700 for some individual cases are impacted by the size of this radius, distributions shown later in Section 3d were found not to be sensitive to the choice of radius, with similar results using 1000 km instead of 500 km (not

shown). For GV500, the minimum value is computed within the 500 km radius, as negative values represent cyclonic activity that is of potential interest for severe wind events, while maximum values are computed for GradT700, which represents strong synoptic-scale fronts. Before the calculation of both quantities, ERA5 data is re-gridded to 1-degree latitude-longitude spacing using a spatial mean, to focus the analysis on large-scale systems. The synoptic conditions for each event will be analysed by inspection of the joint GradT700-GV500 distribution across events and locations. As for the convective environment (Section 2e), GV500 and GradT700 are also computed climatologically for ordinary convective occurrences (based on lightning as a proxy indicator) and non-convective occurrences from 6-hourly ERA5 data during the period 2005-2018, with values for SCW events here compared to each climatological distribution.

3. Results

a. Radar, lightning and station observations

The majority of SCW events show a transient spike in gust intensity compared with the background surface wind gusts (Figure 3). These large, transient gust events therefore correspond to relatively large peak-to-mean wind gust ratios (see Section 2d for definition of this ratio). Large peak-to-mean wind gust ratios were used by Holmes et al. (2018) to define convective wind events in southern Australia, with a threshold value of two applied to both pre and post-event ratios. Events with low peak-to-mean wind gust ratios tend to be confined to the southern coastal locations of Sydney and Melbourne (Figure 3m.a, s.a, s.b, s.c, s.d, s.h), noting that a significant portion of severe weather in these regions tends to be driven by synoptic-scale systems such as midlatitude cyclones and fronts that can produce sustained occurrences of strong surface wind speeds. For events with large peak-to-mean wind gust ratios, the post-event gust intensity tends to either revert back to pre-event conditions (for example, Figure 3m.c, b.f), or remain strong (for example, Figure 3s.e, w.g). The latter type of gust evolution likely represents a change in synoptic air-mass, with convection along a frontal boundary leading to the peak gust, followed by strong post-frontal winds, as described and classified as "transition" events by Spassiani and Mason (2021).

The amount of lightning associated with these cases varies regionally, with Brisbane events associated with much higher amounts of lightning than events in other locations. The number of lightning strokes within 50 km of each event across all locations ranges from 0 to 1,047 during the

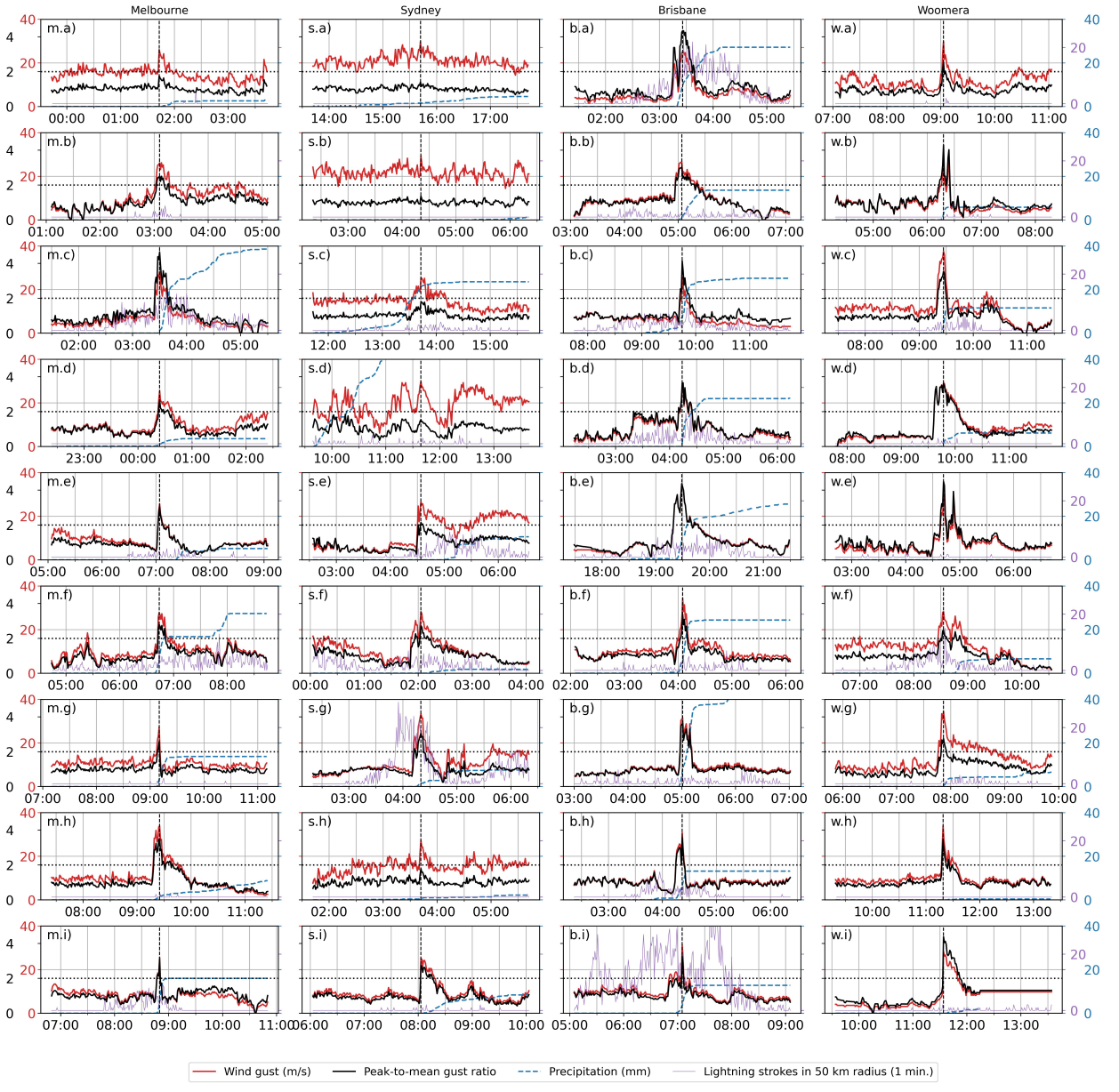

FIG. 3. One minute gust observations in m/s (red line), peak-to-mean wind gust ratio (black line), the number of lightning strokes at one-minute frequency within 50 km of each gust (purple line) and accumulated rainfall in mm (dashed blue line) for each SCW case in Melbourne (m.a-m.i), Sydney (s.a-s.i), Brisbane (b.a-b.i) and Woomera (w.a-w.i). Times are in UTC. A wind gust ratio of two is indicated with a horizontal black dotted line.

hour centred on the peak gust, suggesting that while SCWs are often accompanied by lightning, they can sometimes occur with very little or no lightning during the hour of the peak gust intensity. While these events were defined by Brown and Dowdy (2021a) based on the occurrence of lightning over

a 6-hour period (Section 2a), the results here using higher-resolution data are intended to provide perspectives on lightning occurrences using time scales more relevant for thunderstorms at point locations (one-hour in a 50 km radius). SCW events that occur without lightning during an hour of the peak gust (five events within this set of cases: three in Sydney, one in each of Woomera and Melbourne) are likely related to shallow convection, and this will be explored further in Section 3d.

Radar reflectivity images for each SCW event are shown in Figures 4–7, suggesting that these events may be produced by a wide range of parent storms, as demonstrated by previous studies for other regions of the world (Smith et al. 2012; Gatzen 2013; Yang and Sun 2018; Pacey et al. 2021). These include large linear systems (e.g. Figure 5i), small isolated cells (e.g. Figure 7g), clusters of cells (e.g. Figure 7c), or systems with disorganised, shallow convection (e.g. Figure 4a). Most of these parent storms produce at least some rainfall associated with the SCW event, with 30 out of the 36 cases having the AWS measure at least 1 mm in the hour after the peak wind gust (Figure 3). Like lightning, the amount of rainfall accompanying the SCW events varies regionally. For example, Brisbane events are associated with much higher rainfall totals than other locations, while precipitation is limited for some Woomera cases (Figure 3 w.e, w.h). Using the storm object properties described in Section 2b and presented in Table 1, we attempt to define a classification scheme for these storms that can be applied objectively, by using methods described in the following paragraph, broadly following previous classification schemes (Gallus et al. 2008; Smith et al. 2012; Hitchcock et al. 2021).

In line with Hitchcock et al. (2021) who study rainfall for Melbourne, if the major axis of an object is longer than 100 km and the object has an aspect ratio greater than three, the storm is classified as linear. If the object is longer than 100 km and has an aspect ratio less than three, it is classified as non-linear, broadly corresponding to the objects identified by Gallus et al. (2008). If the object is less than 100 km in length then the storm is either classified as cellular or a cell-cluster, based on the number of local reflectivity maxima within the object (cellular = 1, cell-cluster > 1). For locations where azimuthal shear data are available (that is, events measured with the Melbourne, Sydney, and Amberley AWS), storms are able to be classified as potential supercells by identifying high values of this quantity. If these potential supercells are embedded within a large system (linear or non-linear), then the object is classified as an embedded supercell, to reflect uncertainties

relating to the physical processes leading to the measured gust. If the potential supercell is not embedded within a large system (the object length is less than 100 km), then it is classified simply as supercellular. Here, azimuthal shear values exceeding 0.0040 s^{-1} (after processing described in Section 2b) are considered to be suggestive of a potential supercell, with this threshold chosen based on the distribution across all parent thunderstorms (shown in the Appendix Figure A1), manual inspection of Doppler velocity signatures (see Supplementary Material), and knowledge of historically significant cases within this study exceeding this threshold (for example, see Allen (2012) for Figure 4f). Cases here that exceed this threshold also have high azimuthal shear values through a relatively deep layer (shown in the Appendix Figure A2), suggesting deep rotation consistent with supercellular definitions. Based on evidence available for the SCW cases here, this approach of using a threshold on azimuthal shear is considered suitable for an objective indication of likely supercell events. However, it is noted that in general, the application of this method could potentially exclude some marginal supercell events, as well as events with relatively shallow or narrow rotation (Richter 2007). For events measured at locations without azimuthal shear data (Woomera and Oakey AWS), supercell classifications are not considered as this objective method can't be applied, although some events measured by Oakey AWS could potentially be supercellular based on reflectivity images (Figure 6).

Application of this classification method to the cases here results in 3 linear systems, 13 non-linear systems, 7 cell clusters, 4 supercells, 5 embedded supercells, and 4 cellular storms (Table 1). Table 1 also reveals that several of these storms are relatively shallow, according to the maximum height of the object. There is a bimodal distribution of maximum heights across all parent thunderstorms, with peaks in frequency at 5–6 km and 11–12 km (shown in the Appendix Figure A1), and 10 relatively shallow storms that reach below a 7 km maximum height. These relatively shallow storms appear at the southern locations of Melbourne, Sydney, and Woomera, and are either cellular storms, cell clusters, or non-linear storms. Linear systems also tend to appear in these southern locations, noting a relatively small sample size of linear systems here. Non-linear storms appear most frequently in Sydney, Brisbane and Woomera. Of the 9 storm objects with rotation (supercells and embedded supercells), four occur in Brisbane (as measured by Amberley AWS), two occur in Sydney, and three occur in Melbourne. Of the seven cell clusters identified, three occur at Woomera, one occurs in Brisbane, two occur in Melbourne, and one

occurs in Sydney. Cellular storms either appear in Woomera (three events) or Sydney (one event), again with a relatively small sample size for this storm type.

Although the classifications developed here have been designed to reduce errors in labelling these parent storms compared with manual analysis, misclassifications may still exist due to the automatic segmentation methods described in Section 2b. These misclassifications may relate in some cases to reflectivity regions identified as storm objects that are inconsistent with physical understanding. For example, the event shown in Figure 4h is labelled as non-linear based on having a broad region of high reflectivity values (above 30 dBZ) with a low aspect ratio (Table 1), but with linear orientation at the leading edge of the system suggesting a linear convective system. There is also uncertainty related to the target of the segmentation algorithm in some cases, and whether individual convective cells should be identified as parent objects, compared with the larger, mesoscale convective structure in which the cells are embedded. The choice of identifying individual convective cells here (for example, Figure 5h) could potentially overlook mesoscale structures associated with SCWs.

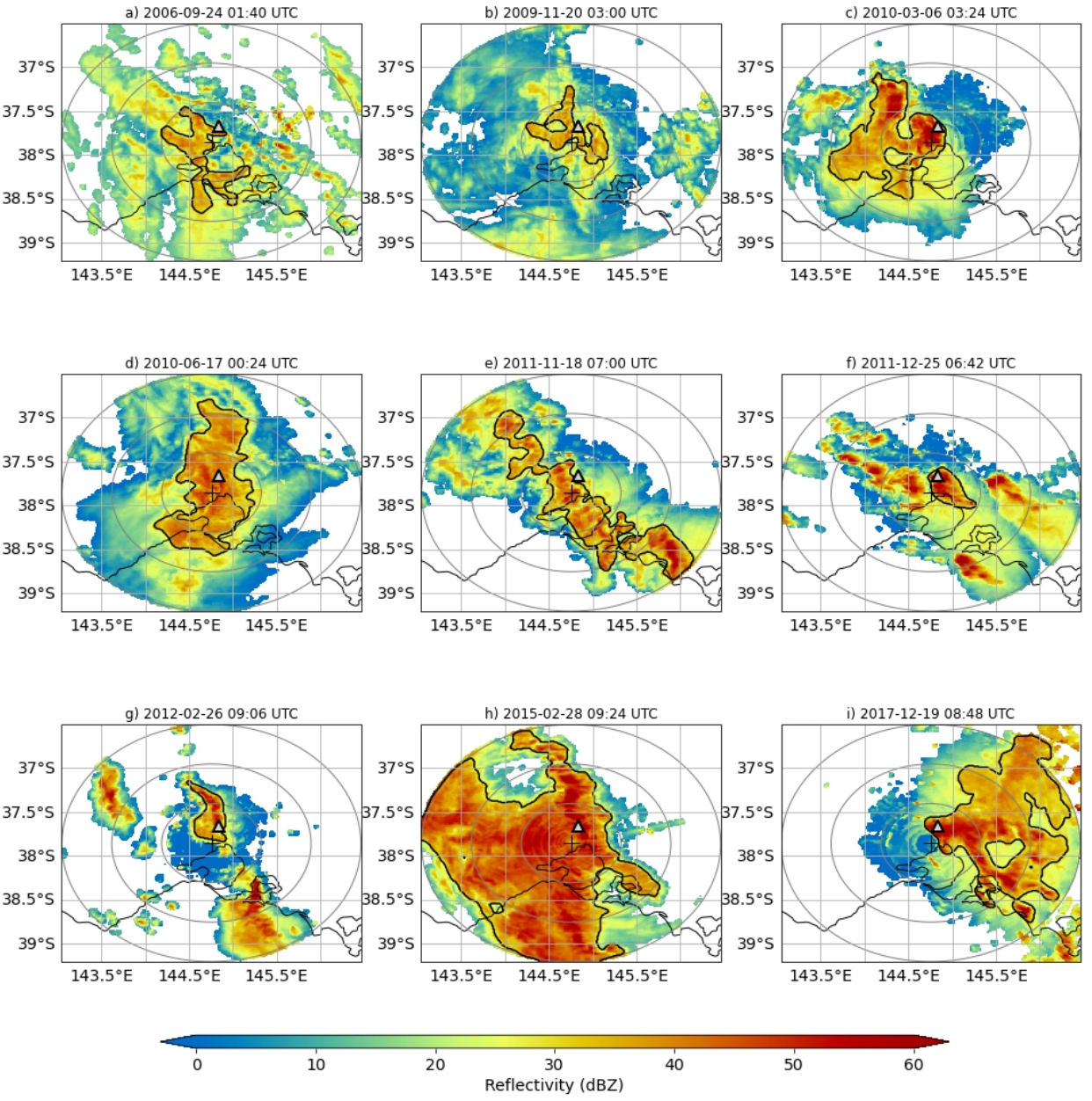

427 FIG. 4. Column-maximum reflectivity for the nine SCW events from Melbourne (Melbourne Airport AWS,
428 marked with a grey triangle), from the Melbourne radar (shown with a "+" symbol"). The most recent scan
429 before each gust is presented, with the parent storm object outlined in black. Range rings of 50, 100, and 150
430 km are shown.

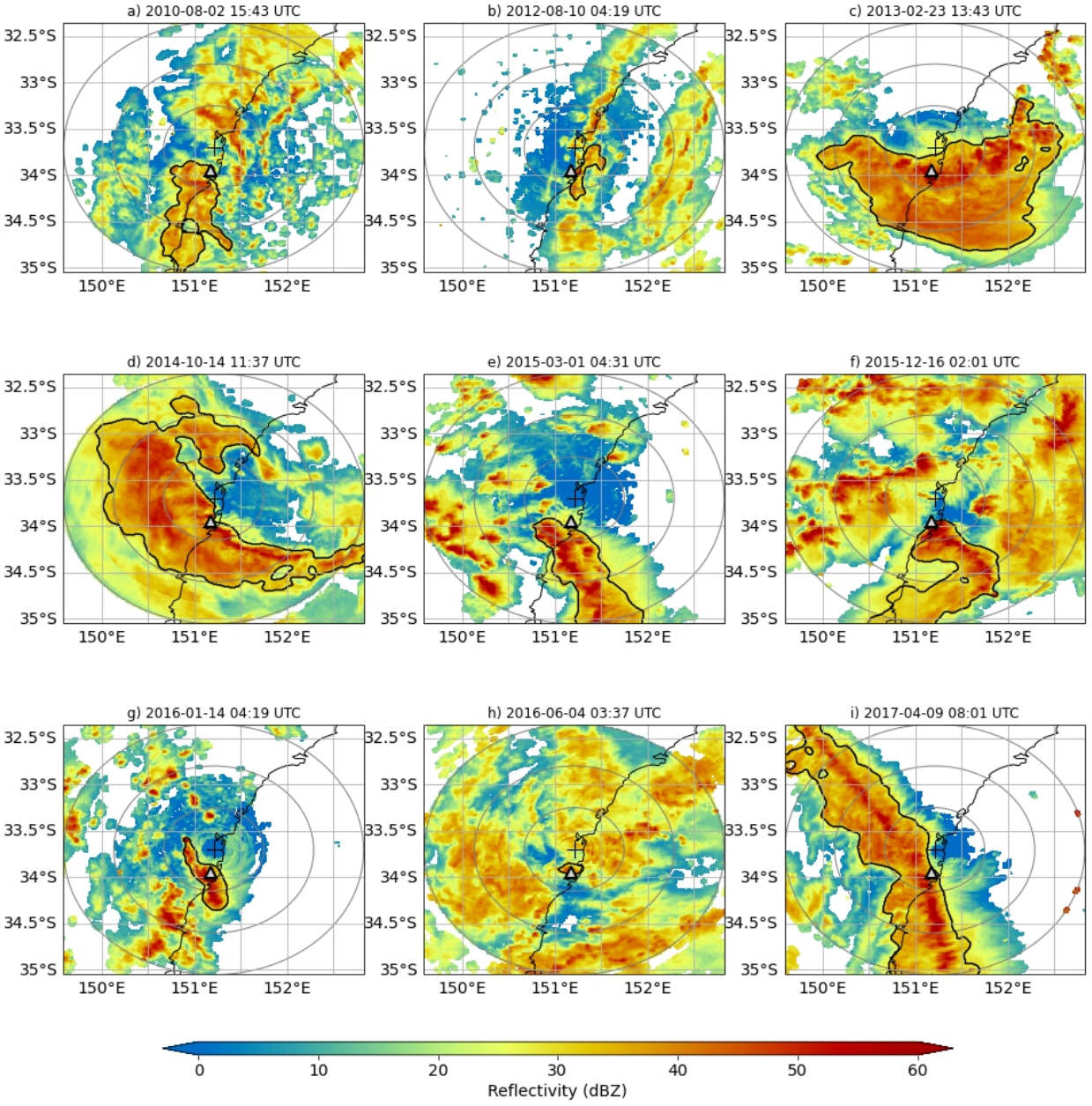

FIG. 5. As in Figure 4 but for Sydney (Sydney Airport AWS)

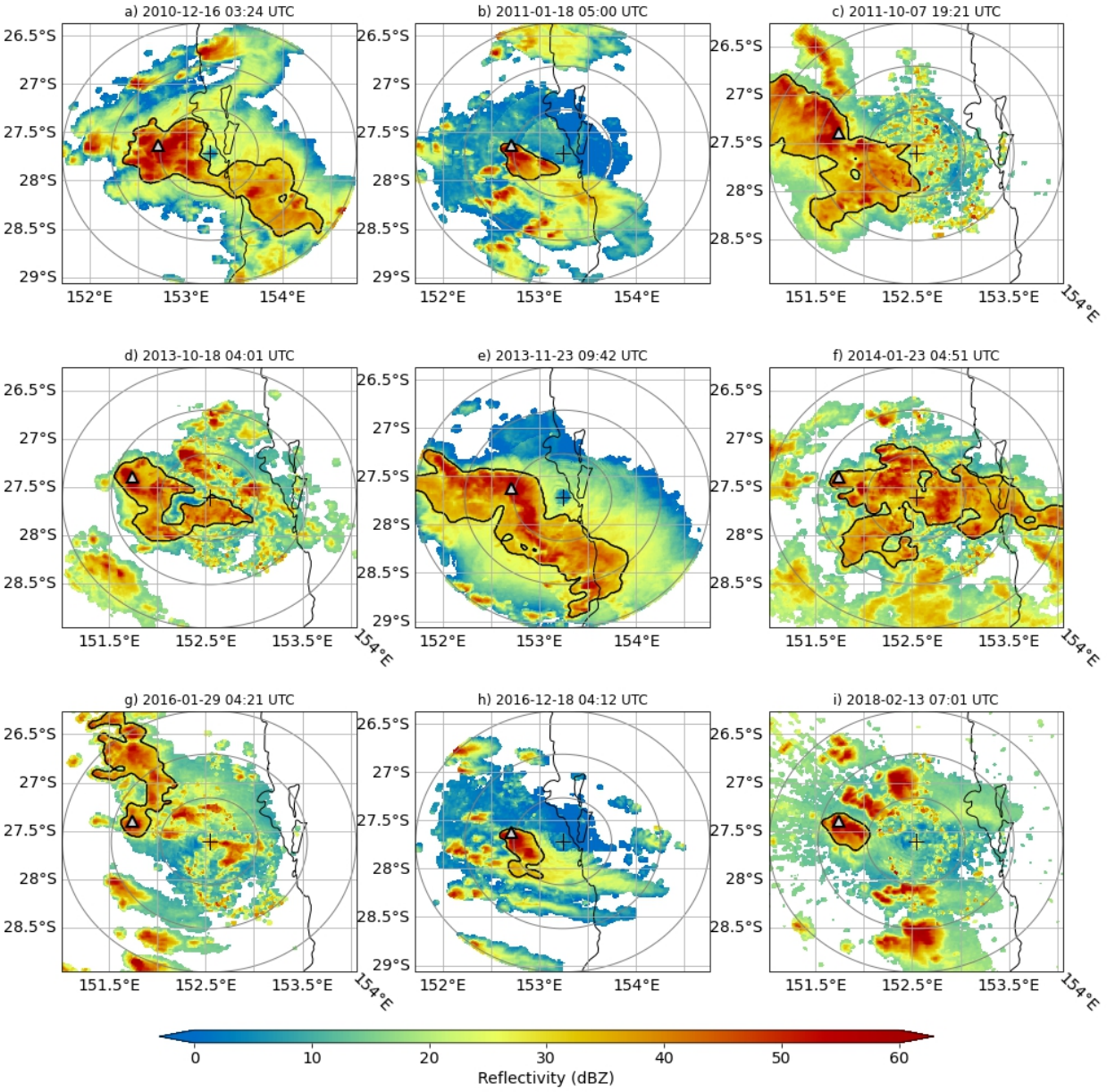

431 FIG. 6. As in Figure 4 but for Brisbane (a, b, e, h Amberley AWS and c, d, f, g, i, Oakey Aerodrome AWS).
432 Note that the Mt. Stapylton radar location is shown for events measured by Amberley AWS, while the Marburg
433 radar location is shown for Oakey Aerodrome AWS.

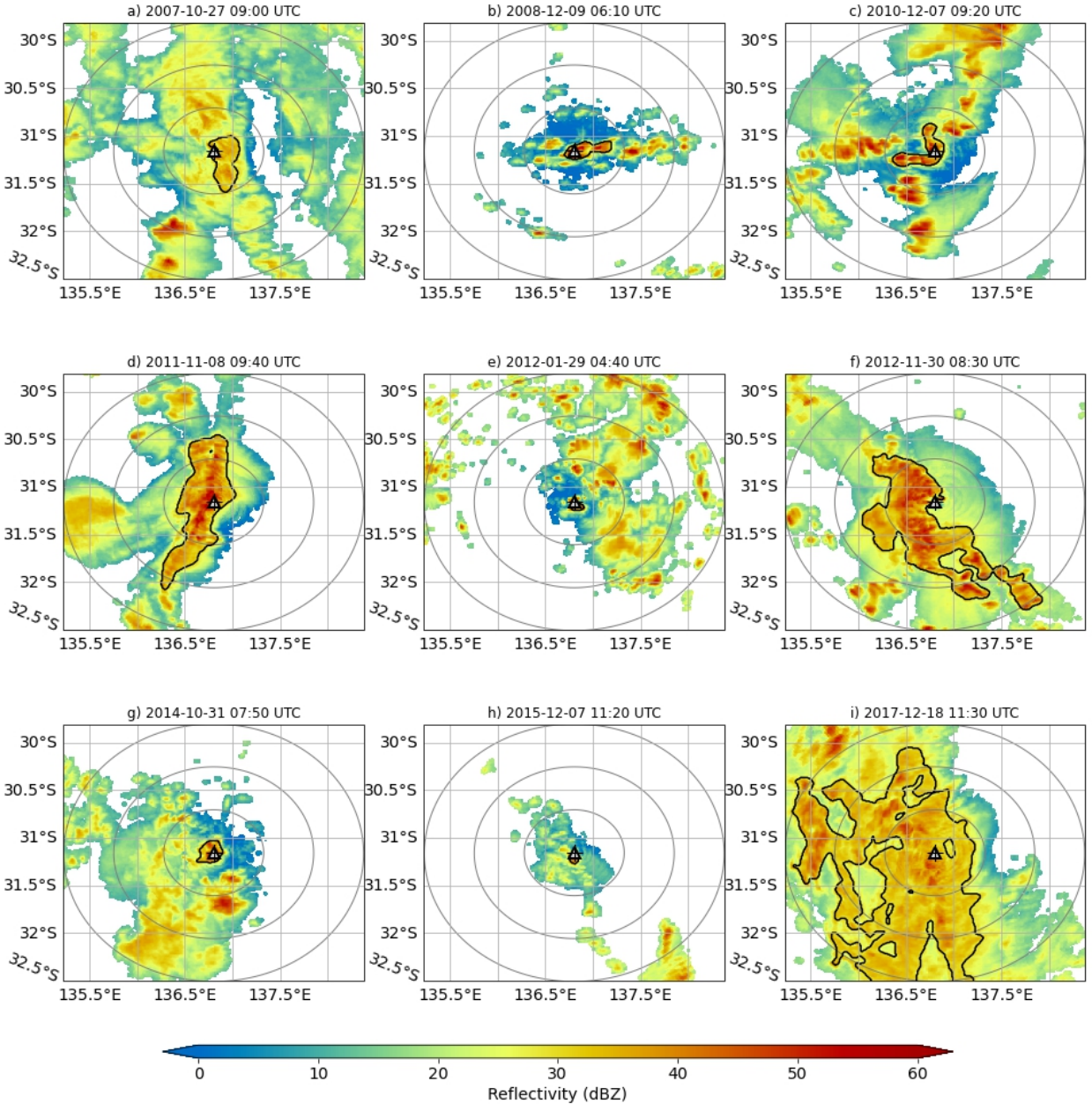

FIG. 7. As in Figure 4 but for Woomera (Woomera Aerodrome AWS)

Time (UTC)	Location (Figure reference)	Major axis (km)	Aspect ratio	Local maxima	Aziumthal shear (s^{-1})	Maximum altitude (km)	Storm type	Environ. cluster
2006-09-24 01:40:02	Melbourne (4a)	142.8	2.4	10		5.0	Non-linear	1
2009-11-20 03:00:32	Melbourne (4b)	97.5	1.5	10	0.0024	6.5	Cell cluster	2
2010-03-06 03:24:32	Melbourne (4c)	141.4	1.4	11	0.0044	11.0	Embedded supercell	3
2010-06-17 00:24:28	Melbourne (4d)	203.3	2.8	12	0.0025	4.0	Non-linear	1
2011-11-18 07:00:35	Melbourne (4e)	291.7	4.3	18	0.0033	11.0	Linear	2
2011-12-25 06:42:36	Melbourne (4f)	60.0	2.1	1	0.0047	13.0	Supercellular	3
2012-02-26 09:06:32	Melbourne (4g)	76.6	2.4	3	0.0025	9.5	Cell cluster	3
2015-02-28 09:24:34	Melbourne (4h)	274.9	1.4	55	0.0028	8.5	Non-linear	2
2017-12-19 08:48:28	Melbourne (4i)	211.5	1.7	26	0.0042	13.5	Embedded supercell	2
2010-08-02 15:43:01	Sydney (5a)	137.6	2.5	12	0.0029	4.5	Non-linear	1
2012-08-10 04:19:02	Sydney (5b)	76.7	3.6	3	0.0025	3.5	Cell cluster	1
2013-02-23 13:43:04	Sydney (5c)	228.4	1.5	31	0.0031	12.0	Non-linear	3
2014-10-14 11:37:05	Sydney (5d)	290.5	1.8	33	0.0032	7.5	Non-linear	1
2015-03-01 04:31:04	Sydney (5e)	162.1	3.1	8	0.0043	11.5	Embedded supercell	3
2015-12-16 02:01:03	Sydney (5f)	146.9	1.5	12	0.003	10.5	Non-linear	3
2016-01-14 04:19:00	Sydney (5g)	89.9	3.5	3	0.004	15.0	Supercellular	3
2016-06-04 03:37:03	Sydney (5h)	22.8	1.9	1	0.003	3.5	Cellular	1
2017-04-09 08:01:00	Sydney (5i)	370.5	4.7	33	0.0031	12.0	Linear	2
2010-12-16 03:24:30	Amberley (6a)	245.3	3.4	16	0.0054	15.5	Embedded supercell	3
2011-01-18 05:00:22	Amberley (6b)	60.7	1.9	2	0.0051	11.0	Supercellular	3
2011-10-07 19:21:46	Oakey (6c)	204.5	2.1	19		11.0	Non-linear	3
2013-10-18 04:01:52	Oakey (6d)	142.5	1.8	8		10.5	Non-linear	3
2013-11-23 09:42:35	Amberley (6e)	269.3	3.3	18	0.005	13.5	Embedded supercell	3
2014-01-23 04:51:49	Oakey (6f)	230.3	1.9	28		10.0	Non-linear	3
2016-01-29 04:21:52	Oakey (6g)	149.2	2.3	10		16.0	Non-linear	3
2016-12-18 04:12:47	Amberley (6h)	62.8	1.7	4	0.0059	12.5	Supercellular	3
2018-02-13 07:01:55	Oakey (6i)	50.6	1.6	2		16.5	Cell cluster	3
2007-10-27 09:00:02	Woomera (7a)	68.3	2.7	3		6.0	Cell cluster	2
2008-12-09 06:10:02	Woomera (7b)	51.0	3.3	2		8.0	Cell cluster	3
2010-12-07 09:20:02	Woomera (7c)	63.5	1.6	5		9.0	Cell cluster	2
2011-11-08 09:40:01	Woomera (7d)	183.5	3.9	12		9.5	Linear	2
2012-01-29 04:40:01	Woomera (7e)	13.1	1.4	1		5.5	Cellular	3
2012-11-30 08:30:01	Woomera (7f)	226.1	2.6	16		13.5	Non-linear	3
2014-10-31 07:50:05	Woomera (7g)	27.6	1.3	1		5.5	Cellular	2
2015-12-07 11:20:04	Woomera (7h)	10.3	1.3	1		5.0	Cellular	2
2017-12-18 11:30:02	Woomera (7i)	272.2	1.6	56		10.5	Non-linear	2

TABLE 1. Object properties for parent storms of each SCW event, as described in Section 2b, as well as the corresponding environmental cluster (see Section 3d for cluster descriptions). Recall that Brisbane events are split between Amberley and Oakey AWS sites (Section 2c). Figures showing reflectivity images are referenced after each location in the table.

b. Convective environment

Values of Qmean01 and S06 from ERA5 for each SCW event are shown in Figure 8, along with the climatological joint probability distribution for these values. Climatological analysis reveals that ordinary convective-environment probabilities (based on lightning occurrences) are shifted to higher values of Qmean01 (mean of 11.0 g/kg) than non-convective environments (mean of 7.7 g/kg) at all locations, associated with increased moisture for deep convection. Ordinary convective-environment probabilities are also shifted to slightly higher values of S06 (mean of 17.9 m/s) relative to non-convective environments (mean of 17.3 m/s).

SCW environments are generally shifted to higher values of Qmean01 and/or S06 (mean of 11.4 g/kg and 22.0 m/s, respectively) compared with ordinary convective environments. There is a slight negative correlation between Qmean01 and S06 for the SCW events examined here (Pearson coefficient of -0.35), suggesting that events with high amounts of low-level moisture tend to occur with relatively low amounts of vertical wind shear, and vice-versa. The climatological Qmean01-S06 distribution shows regional variations for these locations, with Melbourne and Woomera having ordinary convective occurrence probabilities with higher S06 than other locations, while Sydney and Brisbane have higher values for Qmean01. This is consistent with higher amounts of baroclinicity at higher latitudes leading to increased vertical wind shear, and higher amounts of moisture at lower latitudes.

The climatological joint probability distribution for LR13 and Umean06 from ERA5 data is shown in Figure 9, along with values for the SCW events considered here. Results demonstrate a shift to higher values of LR13 for ordinary convective environments (mean of 7.0 K/km) and SCW environments (mean of 7.6 K/km), compared with non-convective environments (mean of 5.5 K/km), consistent with increased instability for deep convection and intense downdrafts. There is also a shift towards higher values of Umean06 for SCW environments (mean of 14.7 m/s) compared with ordinary convective environments (mean of 9.2 m/s) and non-convective environments (mean of 8.9 m/s). For Melbourne and Woomera, SCW events are generally shifted to higher values of LR13 and/or Umean06 compared to ordinary convective environments for these locations. For Brisbane and Sydney, ordinary convective-environment probabilities are generally shifted to higher values of LR13 compared to non-convective environments, although Umean06 is less important for distinguishing between these occurrences. However, Umean06 does appear to provide favourable

conditions for some SCW events in these locations, based on having higher values than ordinary convective environments.

These results demonstrate that environmental values of low-level moisture and vertical wind shear are relevant for SCW occurrences in these locations for eastern Australia. High values of vertical wind shear may be related to SCW event occurrence through an enhanced frequency of organised convection in some cases (Weisman and Klemp 1982), but could also represent high amounts of baroclinicity and synoptic-scale forcing that are known to drive some wind events (Ludwig et al. 2015). The low-level temperature lapse rate appears to discriminate between ordinary convection and non-convective environments at these locations, likely related to greater convective instability, but may only be relevant for the majority of SCW events in Melbourne and Woomera (Figure 9). Deep-layer mean wind speeds discriminate between ordinary convection and SCW occurrences for a subset of events at all locations, potentially related to the mixing of high wind speeds aloft down to the surface (Geerts 2001).

c. Synoptic conditions

For all locations analysed here, the distribution of climatological occurrence probabilities for GradT700, calculated from ERA5 data, is shifted to higher values for ordinary convection occurrences compared with non-convective occurrences. This shift is relatively small for Brisbane and Sydney, which have a smaller range of GradT700 compared with the southern locations of Melbourne and Woomera (Figure 10). The shift in GradT700 for ordinary convective occurrences likely reflects enhanced regions of convective initiation associated with synoptic-scale frontal boundaries in many cases. The distribution of GradT700 for SCW events is relatively uniform, although a number of SCW events occur with above-average values compared with the probability distribution for ordinary convective occurrences, representing the presence of a significant large-scale frontal boundary (Figure 10).

There are two Melbourne events (a, d) and four Sydney events (a, b, d, i) that occur with relatively strong synoptic-scale cyclonic activity, with more negative values of GV500 compared with ordinary climatological occurrences. Cyclonic activity appears to be less relevant for events in Woomera and Brisbane. Each of these Sydney events are associated with "east coast low" pressure systems (Dowdy et al. 2019), based on archived analysis charts and event reports from the Bureau

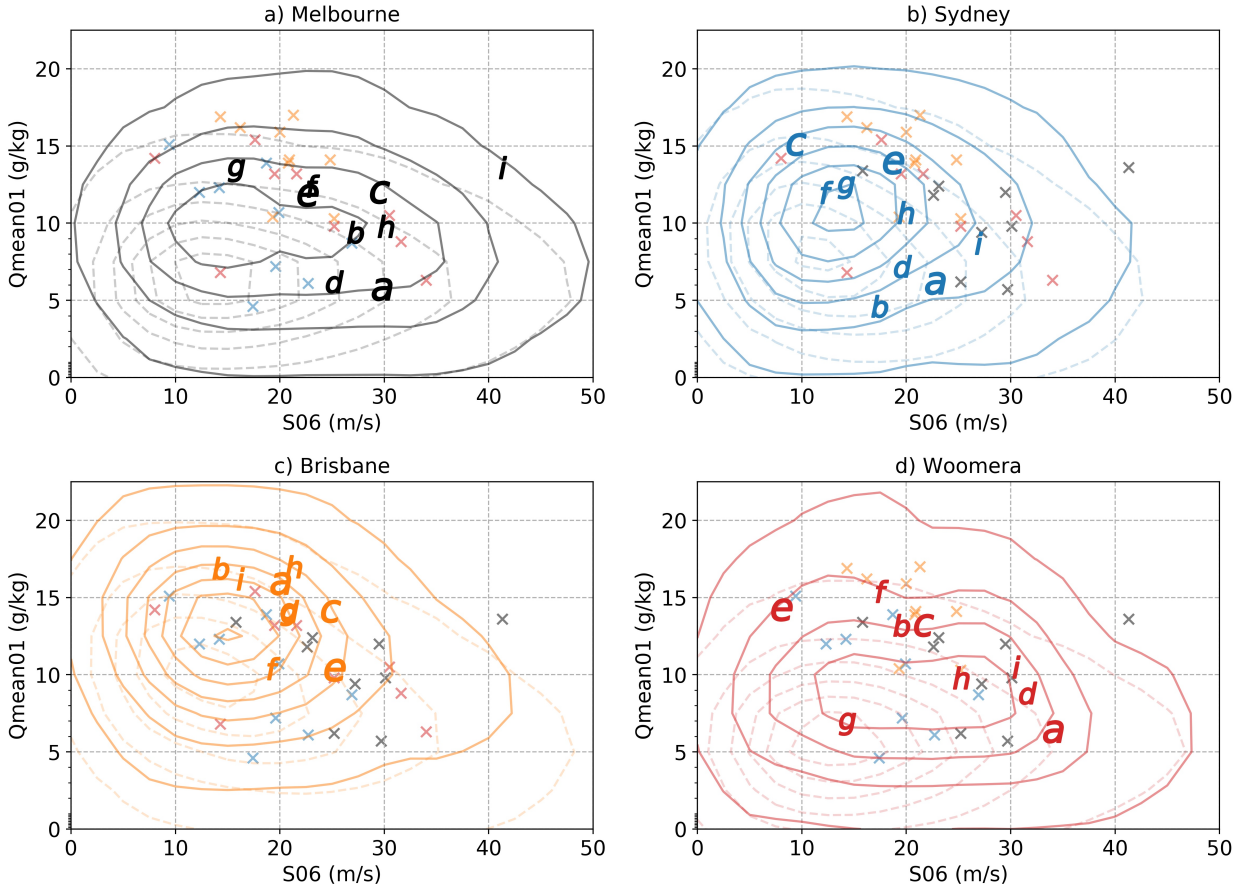

Fig. 8. Qmean01 (g/kg, vertical axis) and S06 (m/s, horizontal axis), as calculated from ERA5 data, for the 9 SCW cases at a) Melbourne, b) Sydney, c) Brisbane and d) Woomera. For comparison, events for each location are marked with the letter corresponding to their panel location in Figures 4–7. For each location, events from all other locations are marked with crosses, including Melbourne (black), Sydney (blue), Brisbane (orange) and Woomera (red). Climatological occurrence probabilities are contoured for reference, using 6-hourly instantaneous gridded data (Section 2e), shown separately for when there is lightning observed in the 6-hourly window centered on those data near the location (solid contour lines) and when there is no lightning (dashed contour lines). Contour levels represent probabilities of 0.001, 0.006, 0.012, 0.018, 0.024, 0.030, and 0.036.

of Meteorology. Maps of GV500 and GradT700 for each SCW event can be found in the in the Supplementary Material.

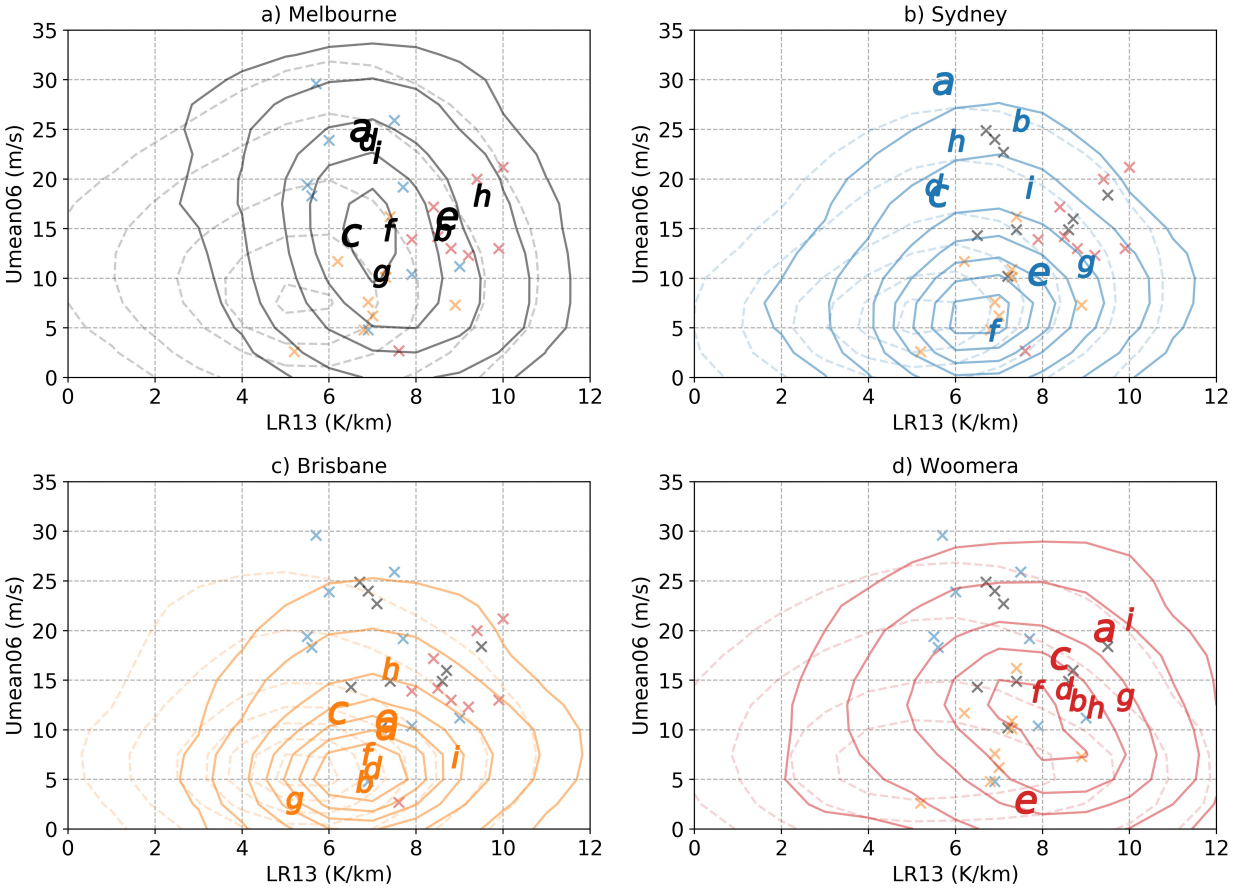

FIG. 9. As in Figure 8 but for LR13 (K/km, horizontal axis), and Umean06 (m/s, vertical axis). Contour levels represent probabilities of 0.001, 0.004, 0.012, 0.02, 0.028, 0.036, and 0.044.

d. Event types

Dominant event types based on the convective environment from ERA5 data are investigated here, based on the four diagnostics analysed in Section 3b, and related to the other statistics presented in Section 3a and 3c including precipitation, hourly lightning strokes, peak-to-mean gust ratio, synoptic features, and parent-storm object properties. K-means clustering was performed with the choice of three clusters, based on results presented in Appendix B.

The resulting three clusters based on the convective environment from ERA5 data are shown in Figure 11 and are characterised by:

- Cluster 1: Low values of Qmean01 and high values of Umean06
- Cluster 2: High values of LR13 and moderate values of Umean06 and Qmean01

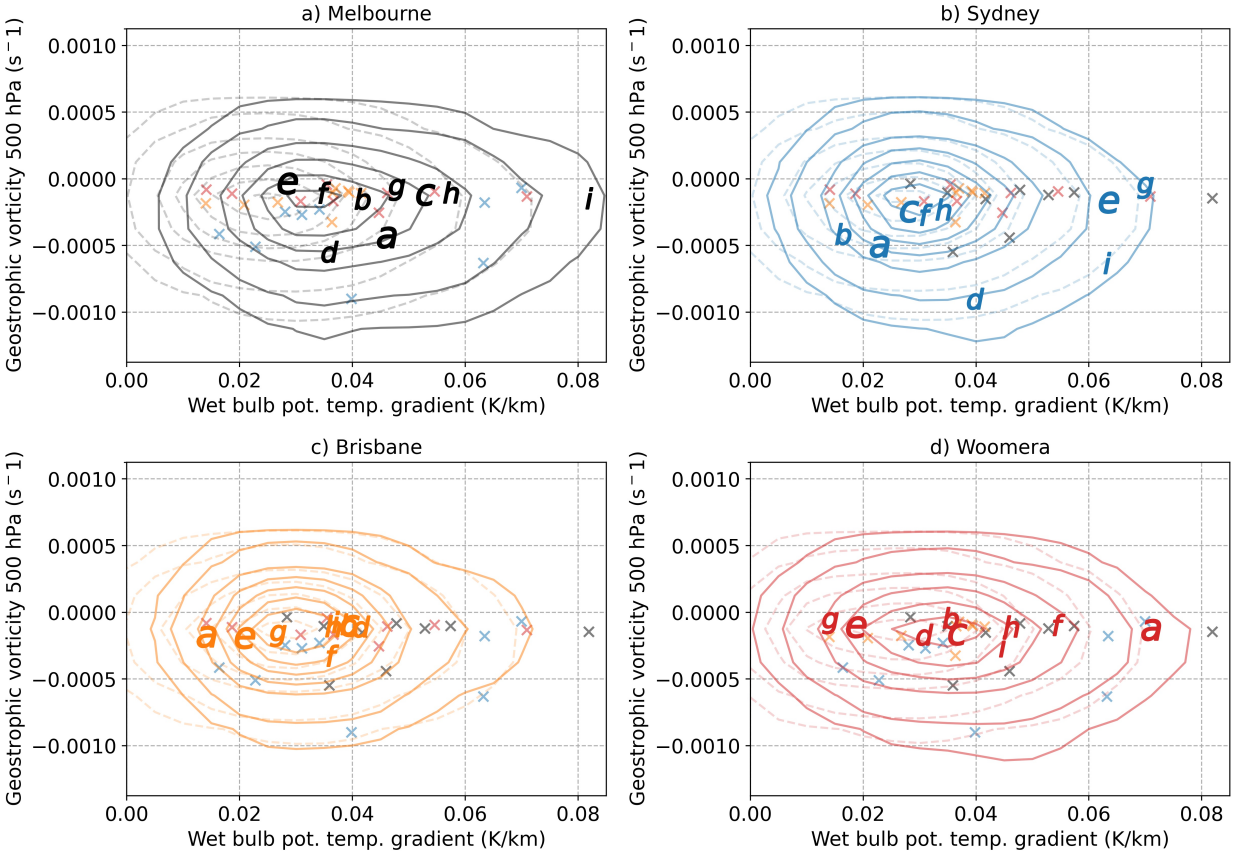

Fig. 10. As in Figure 8 but for the gradient of wet pulb potential temperature at 700 hPa (GradT700), and geostrophic vorticity at 500 hPa (GV500), calculated from ERA5 data, in a 500 km radius around each event. Contour levels represent probabilities of 0.001, 0.004, 0.014, 0.024, 0.034, and 0.054.

- Cluster 3: High values of Qmean01 and low values of Umean06

with these characterisations consistent with clustering using BARRA data (see Appendix, Figure B2). All clusters tend to have relatively high S06, with all but 2 events occurring in environments with S06 greater than 10 m/s, which is often used as a minimum value required for convective organisation (Cintineo et al. 2020; Thompson et al. 2004). However, cluster 1 tends to have relatively high shear values compared to cluster 3, while there appears to be some uncertainty in the cluster 2 shear distribution when considering BARRA results (Figure B2). Cluster 1 is distributed across Melbourne (2 events) and Sydney (4 events), cluster 2 across Melbourne (4 events), Sydney (1 event) and Woomera (6 events), and cluster 3 across Melbourne (3 events), Sydney (4 events), Brisbane (9 events), and Woomera (3 events). There is a significantly higher

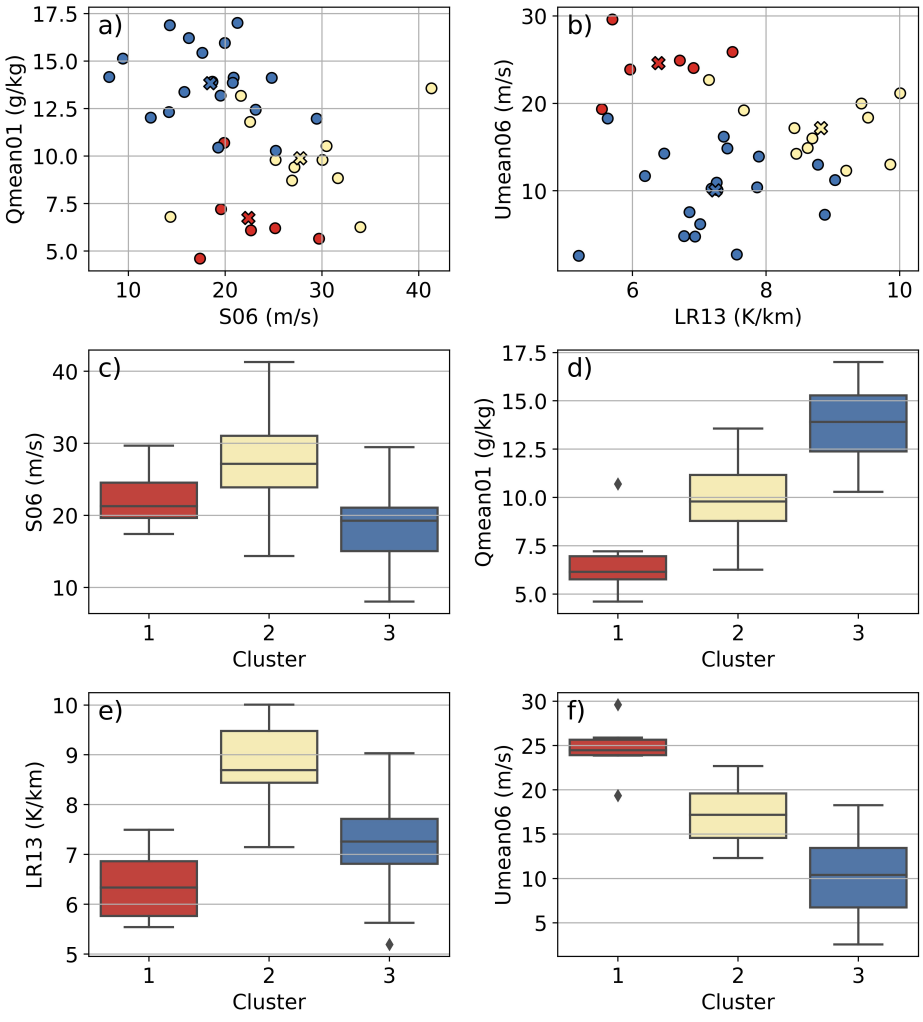

FIG. 11. Three clusters of convective environments for SCW events, resulting from k-means clustering of all 36 events. Events for each cluster are shown in the a) Qmean01-S06 and b) LR13-Umean06 joint distribution, while the distribution of c) S06, d) Qmean01, e) LR13, and f) Umean06 are shown as boxplots for each cluster. Clusters are coloured as follows in increasing order of Qmean01: red (cluster 1), yellow (cluster 2) and blue (cluster 3). Boxes represent the inter-quartile range of the distributions, box whiskers extend to 1.5 times the inter-quartile range, and outliers are shown with black diamonds.

number of cases in cluster 3 (19 cases) than clusters 1 and 2 (6 and 11 cases, respectively) due to all of the Brisbane events belonging to that cluster. However, we found that the clustering of cases was similar when excluding these Brisbane events (not shown).

Distributions of parent-storm size and shape are similar across environmental clusters (Figure 12a–c), although storms within cluster 1 may be slightly more elongated than those in other

clusters based on median values of aspect ratio (Figure 12b). Figures 12e and f suggest that storms occurring in cluster 1 environments tend to be relatively shallow and have low convective pixel fractions compared with other clusters. These storms appear to be strongly associated with synoptic-scale cyclones, as evidenced by the distribution of GV500, resulting in a low peak-to-mean gust ratio due to sustained strong winds (Figure 12g and j). Storms occurring in cluster 2 environments tend to be deeper and more convective than storms in cluster 1 environments, with significantly higher peak-to-mean gust ratios (Figures 12e–g). Storms occurring in cluster 3 environments are the deepest and most convective storms compared with storms in other clusters, and therefore contain most supercells and embedded supercell events identified based on azimuthal shear (Figure 12d–f). Cluster 3 also contains SCW events that occur with relatively large amounts of lightning and precipitation in the hour of the peak gust, compared with clusters 1 and 2 (Figure 12h and i). Similar to cluster 2, high peak-to-mean gust ratios are also produced by cluster 3 events (Figure 12g). Again, these cluster characteristics based on ERA5 data are similar when considering events clustered using BARRA, as shown in the Appendix (Figure B3).

The above analysis relating the convective-environment clusters to storm statistics, surface observations, and synoptic features suggests that the three clusters may correspond to the following physical mechanisms, consistent with current understanding of SCW processes from deep moist convection (Wakimoto 2001) and convection within extratropical cyclones (Earl et al. 2017; Ludwig et al. 2015; Pantillon et al. 2020):

- Cluster 1: Sustained periods of strong winds (Figure 12g), often associated with synoptic-scale cyclones (Figure 12j), and relatively shallow convection (Figure 12e and f).
- Cluster 2: Downbursts and gust fronts driven by evaporation, occurring in environments with steep low-level lapse rates (Figure 11e) and limited low-level moisture (Figure 11d).
- Cluster 3: Deep convective storms (Figure 12f), often with rotation (Figure 12d), producing strong outflow.

The physical meaning of each cluster is investigated further in Figure 13 through the use of composite vertical profiles. Vertical profiles are obtained using ERA5 pressure-level and surface-level data at the most recent hour before each event, vertically interpolated to regular height intervals, at the grid point within 50 km of each event (model land points only) with the highest

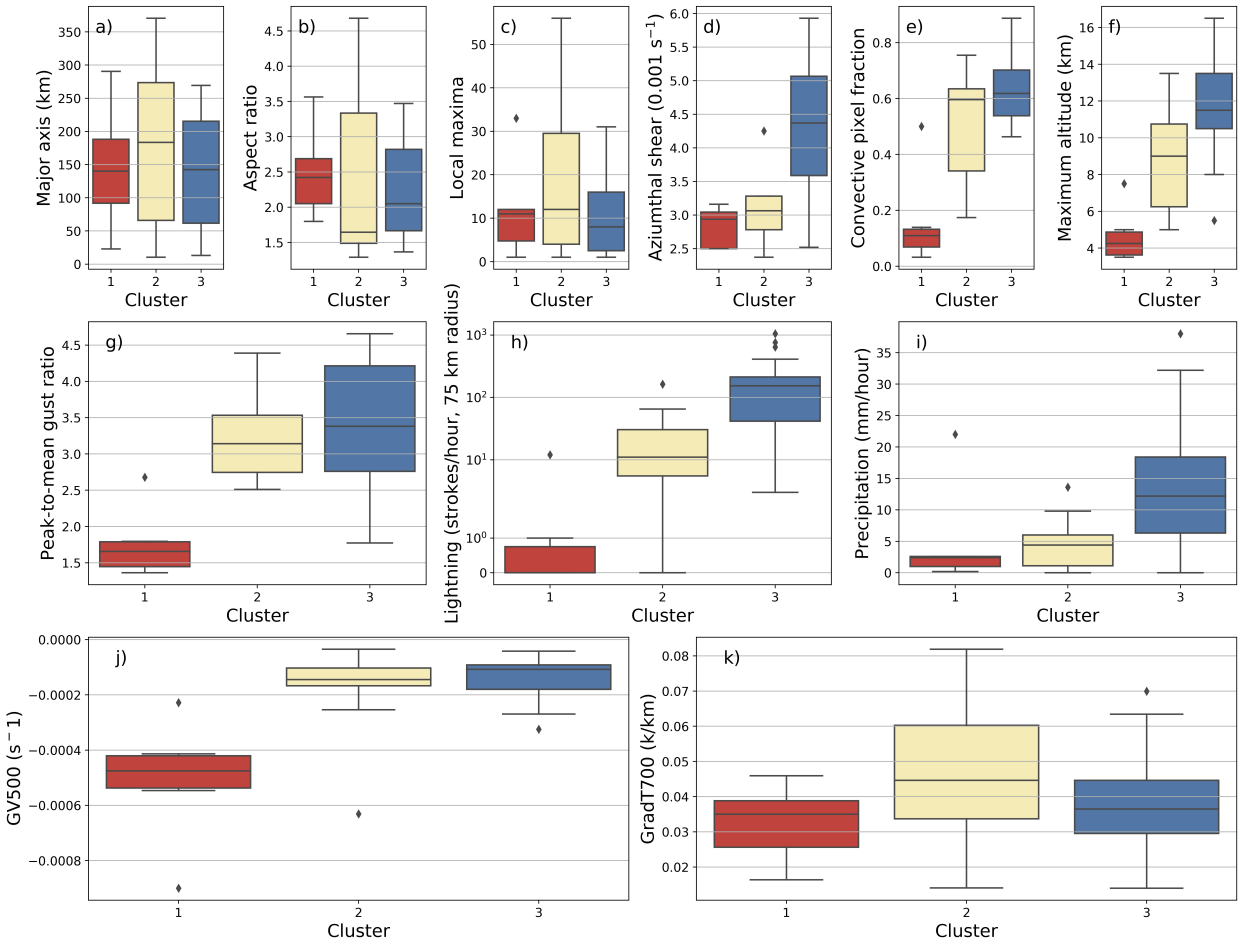

FIG. 12. Distribution of (a–f) storm statistics, (g–i) station and lightning observations (logarithmic scale for lightning strokes), and (j, k) synoptic feature diagnostics for each convective environment cluster. Box and whisker definitions are the same as Figure 11.

value of CAPE (most-unstable parcel, based on having highest CAPE in the vertical). Prior to compositing, each vertical wind profile was rotated such that the mean 0-6 km wind vector is westerly. This was done to ensure that the deep-layer vertical wind speed profile would be broadly preserved after averaging, rather than being smoothed out due to variations in deep-layer wind direction between environments within each cluster. However, it is noted that vertical wind structures within the 0-6 km layer are not expected to be preserved within the compositing process.

Figure 13a shows that cluster 1 has strong winds throughout the lower and middle troposphere, consistent with the distribution of Umean06 in Figure 11. These environments also occur with almost zero most-unstable CAPE, calculated based on the composite most-unstable parcel (32

J/kg), noting that CAPE based on the composite profile for each cluster is towards the lower tail of the distribution across events, due to smoothing of favorable environmental profiles in compositing (see insets in Figure 13). Figure 13b shows that cluster 2 soundings tend to be favourable for microbursts (Wakimoto 1985), with an inverted-V (near-constant potential temperature and mixing ratio) extending from the surface to 800-700 hPa, strong upper-level winds with the potential for horizontal momentum to be transferred down to the surface, and low values of CAPE (263 J/kg based on the most-unstable composite parcel). Figure 13c shows a relatively warm and moist near-surface profile for cluster 3 events, with large amounts of composite-parcel CAPE (1505 J/kg based on the most-unstable parcel) and a moderate amount of vertical wind shear, suggesting the potential for severe, organised thunderstorms (Weisman and Klemp 1982). Reanalysis soundings for individual events are shown in the Appendix separately for each cluster (Figure C1–C3). For events within cluster 3, individual soundings generally suggest relatively warm and moist low-level environments with large CAPE, similar to the cluster 3 composite. However, there are also several events with inverted-V environmental profiles, suggestive of microburst soundings discussed earlier in relation to cluster 2. In addition, some of the cluster 3 events exist within low wind shear environments, which may limit potential for organised thunderstorms (Weisman and Klemp 1982). These findings suggest that although the environmental clusters capture three broad types of SCW events, there still remains significant variation within each cluster.

4. Discussion

Convective environments and synoptic features were examined here for SCW events in eastern Australia. Several clusters of those conditions were found to be indicative of different types of SCW processes. These processes may be produced by different types of storms, including linear systems, large non-linear systems, discrete cells, cell clusters, and supercells, with some of these storms being relatively shallow. Previous studies have shown that the distribution of parent-storm types for SCWs is non-uniform. For example, Klimowski et al. (2003) and Gatzen (2013) found that the majority of events in the northern High Plains of the United States and Germany, respectively, are associated with linear modes including bow echoes, while Pacey et al. (2021) found that European events in warm-season environments are most often produced by cellular convection. Some regional variations are suggested by the current study, including a greater proportion of shallow

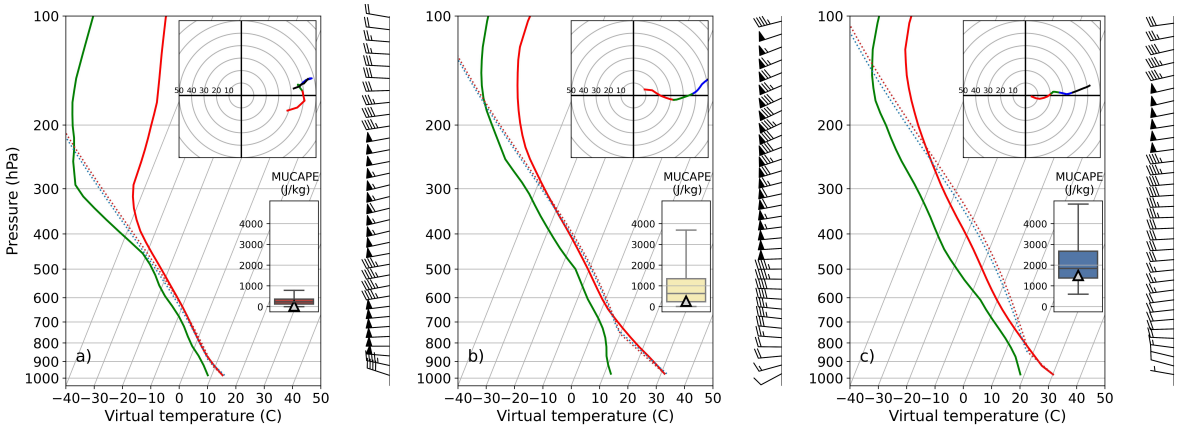

FIG. 13. Composite virtual temperature (red, degrees C), dew point (green, degrees C), and wind profiles (barbs, hodograph, kts) for the convective-environment clusters (a) 1, (b) 2 and (c) 3. Lifted-parcel traces are shown in terms of virtual temperature, and use the composite 100 hPa mixed-layer mean (blue dotted) and most-unstable conditions (dotted red). Hodographs are shown with red, green, blue and black lines representing 0-3, 3-6, 6-9, and 9-12 km winds, respectively. An inset in each figure panel shows boxplot distributions of most-unstable CAPE (MUCAPE) across the events in each cluster, with MUCAPE based on the composite profile represented by a triangular marker. Boxes here represent the interquartile range, whiskers extend from minimum to maximum, and the horizontal line represents the median.

storms occurring in Melbourne, Sydney, and Woomera; however, the sample size of this case dataset is not large enough to draw conclusions on the relative frequency of storm modes. Instead, this study provides illustrative examples of event types across the broad region. The size of the case dataset also does not allow for a thorough assessment of the relationship between the identified storm modes and the environmental clusters defined in Section 3d. However, it is expected that there may be some dependence between the environment and storm morphology based on previous studies (Thompson et al. 2012). In addition, supercell classifications are only possible here for a subset of locations with available Doppler velocity data, limiting analysis of regional variations of that storm type. As an extension of this work, storm classification methods will be applied to a longer dataset at locations with Doppler velocity data available, to gain insights into the variability of SCW-producing thunderstorm types in Australia, and to investigate the relationship between thunderstorm types and environmental clusters.

Different environmental conditions are also associated with significant variations in the number of lightning strokes associated with each SCW event, as well as in the observed gust ratio. While the majority of events are associated with a significant amount of lightning, there are some events that occur with very little or no lightning within an hour of the peak gust. Based on their environmental conditions, these low or no-lightning cases tend to occur within a cluster of events with strong background winds that tend to be in the presence of a strong synoptic-scale cyclone (Section 3d). These events are shown to be generally associated with relatively shallow parent storms, which are less likely to produce deep updrafts reaching temperatures conducive to charge separation processes. These types of events are not included in some definitions of SCWs based on associations with lightning as a proxy for deep moist convection (Mohr et al. 2017; Brown and Dowdy 2021a; Yang et al. 2017; Taszarek et al. 2020a), and future work on SCWs may need to consider other definitions to include events such as these associated with relatively shallow convection, especially for regions where these events tend to occur frequently, such as in southeastern Australia. Damaging wind events in the United States may also be associated with low or zero amounts of lightning, as demonstrated for two derecho events that progressed into environments with low amounts of convective instability (van den Broeke et al. 2005), while shallow convective lines with updrafts generally extending only 3 km above ground level can often produce convective hazards in the United Kingdom, including tornadoes and damaging winds (Clark 2013). A lack of observed lightning associated with some events could be due to detection inefficiencies, with WWLLN having an efficiency of ~10% globally (Virts et al. 2013). This could be particularly relevant prior to 2012 when the size of the detection network was relatively small (Holzworth et al. 2021), although WWLLN accuracy is considered sufficient to enable the detection of most deep convection (Jacobson et al. 2006). In addition, some events examined here produce peak wind gusts with intensities below two times the four-hour mean gust, which has been considered characteristic of a synoptic, rather than convective event in some instances (Holmes et al. 2018). It is possible that while these events occur in the vicinity of convective processes based on lightning within a 6-hourly window (Section 2a), they may not necessarily be driven by convective processes as evidenced by low peak-to-mean wind gust ratios, and future work could potentially incorporate a similar ratio in identifying convective wind events. The temporal characteristics of some events in this study also suggest a transition to a different wind regime after

the peak gust, which was separated from convective gusts by Spassiani and Mason (2021). The above-mentioned points highlight the difficulty in producing a consistent definition of a convective wind gust, outlined in further detail for example by De Gaetano et al. (2014).

The SCW events analysed here appear to be related to high values of environmental low-level moisture, temperature lapse rate, vertical wind shear, and deep-layer mean wind speeds, relative to the climatological distribution at each location. Low-level moisture and vertical wind shear are well established controls on severe thunderstorm occurrences, through providing convective instability and the potential for storm organisation (Weisman and Klemp 1982; Weisman and Rotunno 2004). In addition, steep low-level lapse rates, strong deep-layer mean wind speeds, and high values of near-surface moisture have been found by previous studies to be relevant for SCW gusts, including for Australia (Geerts 2001; Brown and Dowdy 2019, 2021a), and in other regions of the world (Kuchera and Parker 2006; Taszarek et al. 2017, 2020b; Sherburn et al. 2021). However, the events here suggest that the extent to which these are relevant factors may vary regionally in eastern Australia, with steep low-level lapse rate environments potentially less common for Brisbane than for the inland location of Woomera, for example. The skill of each of these environmental diagnostics for event prediction have not been quantified here based on a relatively small sample size, although an assessment of predictive skill could be assessed as part of future work. A small number of SCW events appear to be related to unusually strong synoptic-scale fronts and cyclones that may be associated with regions of enhanced convective initiation, noting that strong winds within these synoptic systems can lead to severe surface winds through vertical transport by convective processes and mesoscale features (Earl et al. 2017).

Through k-means clustering, it is suggested that SCWs in eastern Australia could occur within three convective-environment clusters, with composite soundings for each cluster characterised by low (clusters 1 and 2) and high (cluster 3) amounts of composite-parcel CAPE (Figure 13). This is consistent with findings made by Pacey et al. (2021) for SCW events in Europe, in which events clustered into two environments with high and low amounts of CAPE. Here, composite-parcel CAPE is shown to be greater for clusters with relatively high amounts of low-level moisture. However, low-level temperature lapse rates tend to be significantly steeper for cluster 2 events compared with the high-CAPE cluster (cluster 3). This suggests that for events in cluster 2, steep low-level lapse rates may be associated with severe winds through environmental factors related

to downdraft intensification near the surface and downburst production, rather than by enhanced convective instability. In addition, for environments in cluster 1 (low composite-parcel CAPE), events are characterised by high values of deep-layer mean wind, and are shown to be associated with relatively shallow storms, low peak-to-mean wind gust ratios, and synoptic-scale cyclones. These events are likely similar to European windstorms described by Ludwig et al. (2015) for example, that are associated with convective processes embedded within extratropical cyclones leading to damaging surface winds. Environments within the high-CAPE cluster (cluster 3) are shown to produce most supercellular storms within the dataset, defined by radar-observed rotation. While supercells generally occur in environments with high vertical wind shear, this high-CAPE cluster (cluster 3) tends to have the lowest values of deep-layer vertical wind shear compared to other environmental clusters (Figure 11). It is possible that the relatively strong vertical wind shear in other clusters (clusters 1 and 2) reflects the use of a fixed-layer shear quantity (from 0–6 km above ground level) that ignores storm/inflow depth (compared to effective shear as described by Thompson et al. (2007)). The higher amounts of deep-layer shear in clusters 1 and 2 may also reflect enhanced baroclinicity in the relatively high-latitude locations in which those storms occur (Sydney, Melbourne, and Woomera), although this finding warrants further investigation. In summary, the overall findings discussed here suggest that SCWs in eastern Australia may tend to occur in environments supportive of shallow convective transport of strong synoptic winds from aloft (cluster 1), downbursts (cluster 2), and deep, convective storms including supercells (cluster 3), with each of these processes having been demonstrated to occur in Australia by previous case studies (Sherman 1987; Richter et al. 2014; Earl and Simmonds 2018).

Although the current study has demonstrated the diversity of SCW events in eastern Australia, and suggested three dominant types of convective environment, the frequency of event types and regional variations are uncertain due to a relatively small sample size of 36 cases. In addition, cases have been defined using the dataset produced by Brown and Dowdy (2021a) that may potentially neglect events with limited amounts of lightning in some cases, including for example, events associated with cool-season convection that may be produced by environmental cluster 1. However, it is noted that the majority of SCW events appear to be associated with deep moist convection, and would be identified using this approach based on lightning observations (as discussed in Section 3a). Other observational uncertainties may include the use of AWS to

measure SCW events at a point location, which likely underestimates the peak gust for any given event, and the classification of thunderstorm types using an objective process that may produce some misclassifications as demonstrated in Section 3a. Future work should attempt to use a more robust definition to associate severe wind events with convective processes, such as based on radar information from the AURA dataset (Section 2b), while extending the observational record spatially and temporally to better address variability in SCW event types and parent-storm modes. This will also allow for an assessment of the robustness of the environmental clusters derived here based on a small set of cases, as well as the objective storm classification methods presented in Section 3a.

5. Conclusion

Several different types of severe convective wind (SCW) events have been observed in various regions around the world, driven by a range of physical processes. However, these event types have not been systematically observed in Australia. This study has analysed a range of SCW events in eastern Australia, in terms of their environmental conditions, parent-storm types, and synoptic features. Based on the set of 36 cases examined here, the key findings are:

- SCW events are produced by several different types of storms based on radar-derived statistics. These include linear systems, large non-linear systems, cell clusters, supercells, and cellular storms.
- Low-level moisture, low-level temperature lapse rates, deep-layer mean wind speeds, and vertical wind shear are influential for discriminating non-convective, convective, and SCW occurrences, with potential regional variations in their relative importance.
- Three event types are identified by statistical clustering of convective-environment diagnostics, which are likely driven by shallow vertical transport within strong synoptic systems, downbursts within moderately deep convective storms, and outflow from deep convective storms including supercells.

This type of systematic analysis could be applied to long-term datasets, to determine climatological characteristics of each event type, similar to studies in other regions (Pacey et al. 2021; Smith et al. 2013). The identification of various types of SCWs and their climatological occurrence

frequency is intended to help enable further research and applications building on the results presented here, including potential for understanding future climate change impacts for these events. Current best-estimates of future projections for SCWs in Australia are based on changes in the frequency of convective environments, and have various uncertainties including relating to the wide range of event types with potentially different responses in a warming climate (Brooks 2013; Brown and Dowdy 2021b). Similarly, SCWs provide a challenge for weather forecasting due to the different types of events that can occur (Corfidi 2017). To complement environmental predictions of SCW occurrences, convection-allowing models should also be used, as is increasingly common in weather and climate prediction for thunderstorm hazards (Prein 2015; Sobash et al. 2011). However, these models will need to be assessed in their application to the SCW event types noted here for eastern Australia.

Acknowledgments. AB, TL, and SH are supported by the ARC Centre of Excellence for Climate Extremes (CE170100023). AD is supported by the National Environmental Science Program (NESP). Comments on earlier versions of this manuscript by Rob Warren and Joshua Soderholm from the Bureau of Meteorology are gratefully acknowledged, as well as comments from three anonymous reviewers.

Data availability statement. The Brown and Dowdy (2021a) case dataset is available here: https://doi.org/10.5281/zenodo.4448518. Reanalysis data are openly available from the Australian National Computing Infrastructure (NCI) for ERA5 (http://dx.doi.org/10.25914/5fb115b82e2ba) and BARRA (http://dx.doi.org/10.4225/41/5993927b50f53). AURA is also openly available on NCI (https://dx.doi.org/10.25914/5f4c85732ee80). Information on access to WWLLN lightning data can be found from http://wwlln.net, while information on access to station wind and rainfall observations collected by the Australian Bureau of Meteorology can be found at http://www.bom.gov.au/climate/data/stations/. Plotting of radar images was done using the python ARM Radar Toolkit (Helmus and Collis 2016), and sounding composites were plotted using the Sharppy python package (Blumberg et al. 2017).

APPENDIX A

Parent-storm statistics

For the objective classification of supercells, a threshold is chosen for aziumthal shear. The threshold on azimuthal shear is based on the distribution over parent storms with available data. Figure A1 shows the distribution of azimuthal shear, with clustering above and below 0.0040 s^{-1}. In addition, shallow storms are discussed in terms of the maximum storm altitude. The distribution of maximum storm altitude is shown in Figure A1, with a bimodal distribution and clustering above and below 7 km.

Figure A2 shows the vertical profile and temporal evolution of azimuthal shear for the nine parent storms classified as supercellular or embedded supercells. These results demonstrate that high values of azimuthal shear are relatively long-lived and occur over a deep layer for these storms, consistent with persistent, deep rotation as observed in supercells.

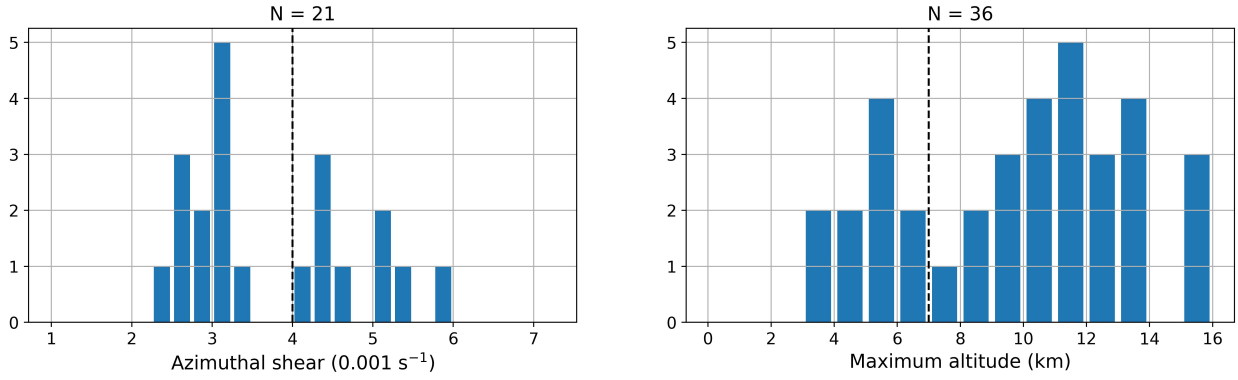

FIG. A1. (left) Histogram showing the distribution of azimuthal shear in parent storms for SCW events and (right) histogram of maximum altitude. The number of samples in each histogram is indicated above the figure panels.

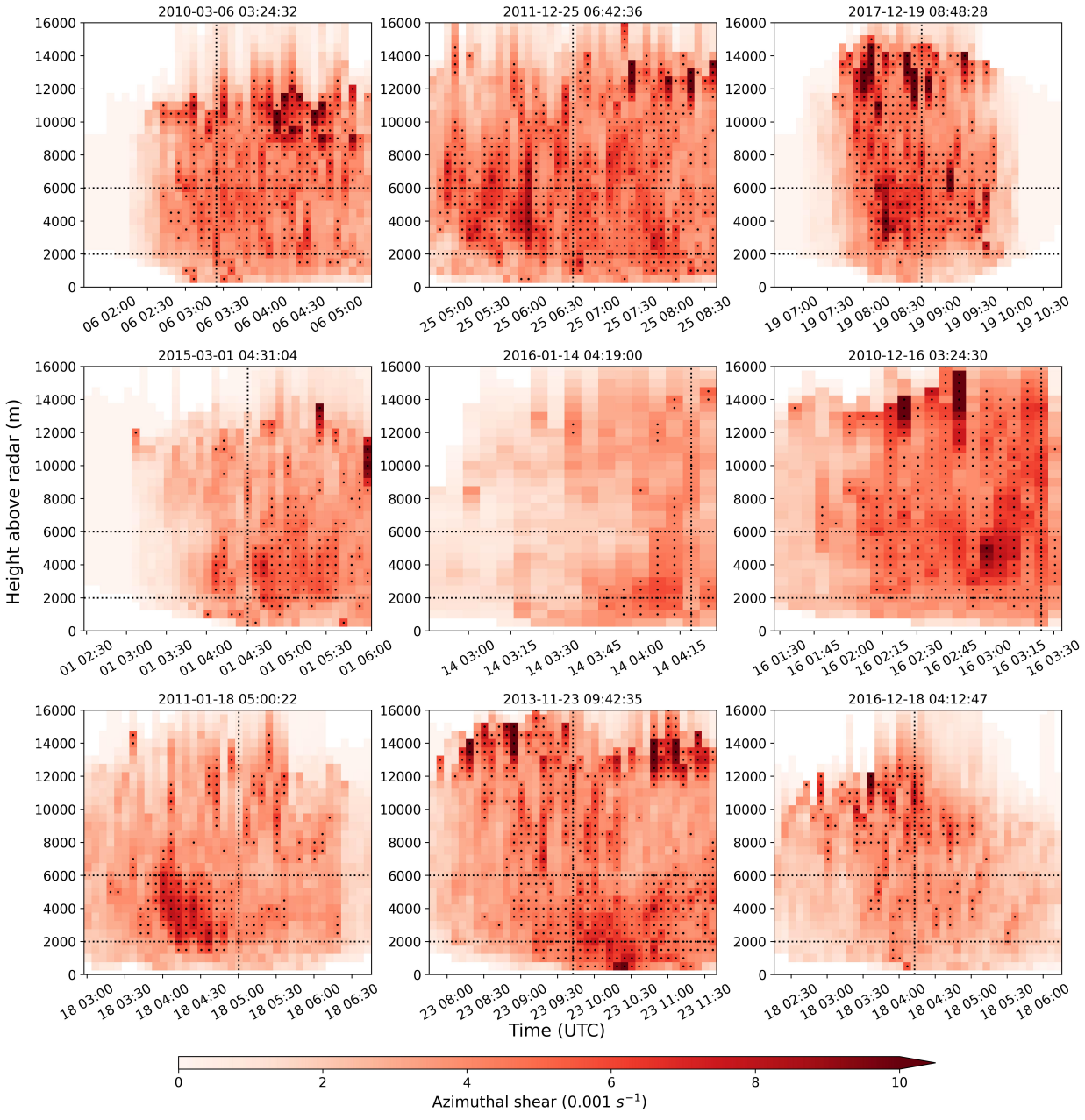

792 FIG. A2. Time-height distributions of azimuthal shear (shading), for all parent storms that exceed the threshold
793 value of 0.0040 s^{-1} for the 99.5th percentile over the 2–6 km layer. This threshold is represented at point locations
794 with black dots. This threshold is used for supercell classifications in Section 3a. Times are shown for up to two
795 hours either side of the peak SCW gust (vertical dotted line), noting that the storm lifetime may be greater or less
796 than those time bounds. Horizontal dotted lines represent the 2–6 km layer above the radar height, over which
797 azimuthal shear is summarised for calculating the storm object properties (Section 2b).

APPENDIX B

Evaluation of statistical clusters

Here, statistical k-means clustering is evaluated in terms of the number of optimal clusters and consistency between reanalysis datasets. The number of clusters is chosen based on an optimal silhouette score, following Zhou et al. (2021) for hailstorm environments. The silhouette score measures how similar each case is to other cases within their own cluster, compared to how similar they are to events from other clusters, with higher scores representing more isolated and compact clusters. An optimal score is reached using three clusters based on both the ERA5 and BARRA reanalysis (Figure B1). The optimal number of clusters is also assessed by comparing how consistent the clustering is when using data from ERA5 and BARRA, separately. This consistency is quantified by the Rand score. For example, a Rand score of 1 would mean that each event is placed in the same cluster using both reanalyses, and the clustering is perfectly consistent regardless of the dataset used. In contrast, a Rand score of zero would mean that all events are placed in different clusters depending on if BARRA or ERA5 data is used, representing perfectly inconsistent clustering. The Rand scores shown in Figure B1 suggests that a choice of three clusters provides relatively consistent clustering of each event between ERA5 and BARRA compared with other cluster amounts. Finally, Figure B2 shows that the distribution of convective diagnostics using BARRA data for clustering is similar to ERA5 data (Figure 11), with minor differences noted in Section 3d, while Figure B3 shows that the distribution of storm statistics, station observations, lightning strokes, and synoptic diagnostics are similar between ERA5 and BARRA clusters.

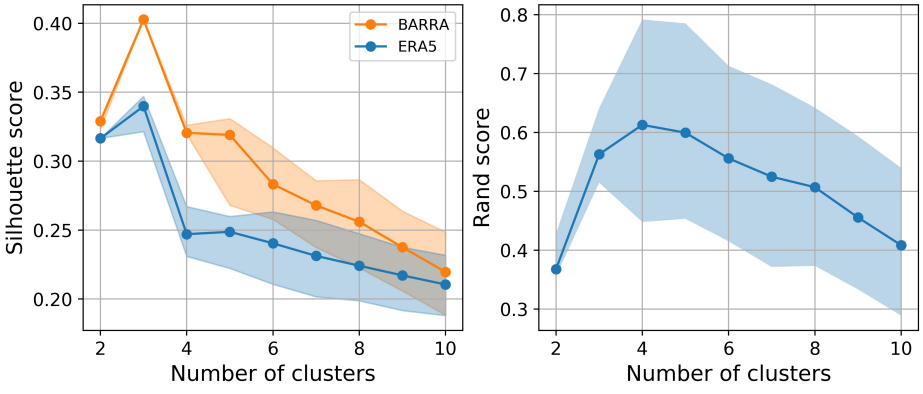

FIG. B1. (left) The silhouette score and (right) Rand score when applying k-means clustering to the convective environment of SCW events, using a range of cluster numbers from 2 to 10, and two separate reanalysis datasets (BARRA and ERA5). The silhouette score measures how similar each case is to other cases within its own cluster, while the Rand score measures the consistency of the clustering when using data from the two different reanalyses. For both scores, clustering is performed 1000 times on a random sample of events with replacement, with the 2.5th–97.5th percentile range shaded.

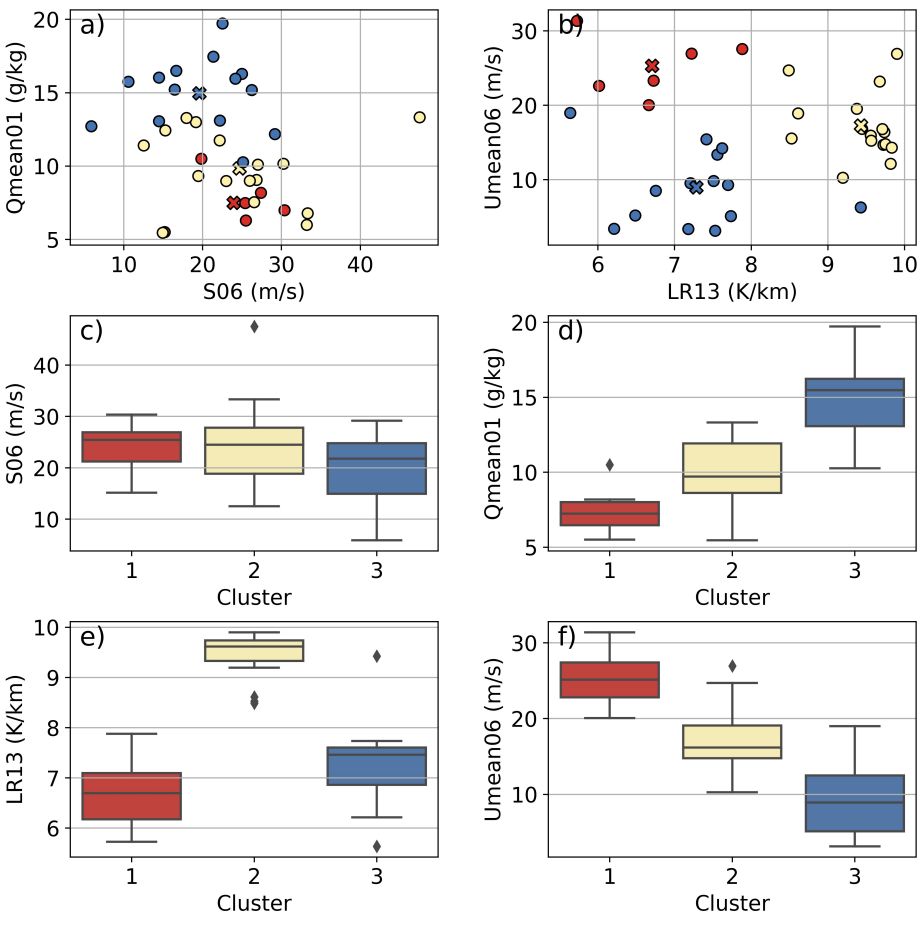

FIG. B2. As in Figure 11 but using environmental data from BARRA

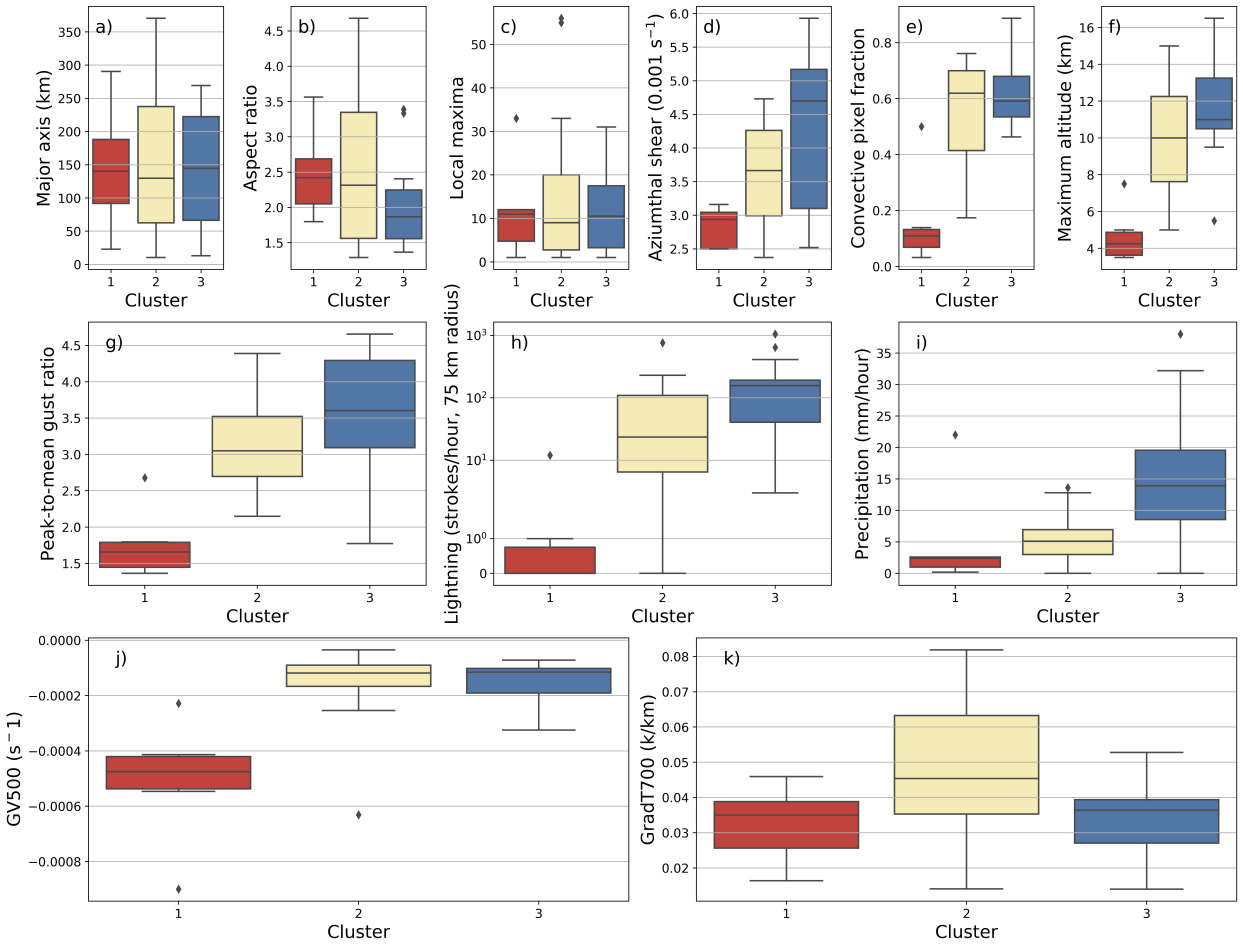

FIG. B3. As in Figure 12 but with clustering from BARRA data

824 APPENDIX C

825 **Environmental soundings for individual cases**

826 Here, reanalysis model soundings are presented individually for each SCW event within cluster
827 1 (Figure C1), cluster 2 (Figure C2) and cluster 3 environments (Figure C3, Figure C4). Sounding
828 methods are discussed in Section 3d, noting that wind profiles for individual soundings here are
829 not rotated.

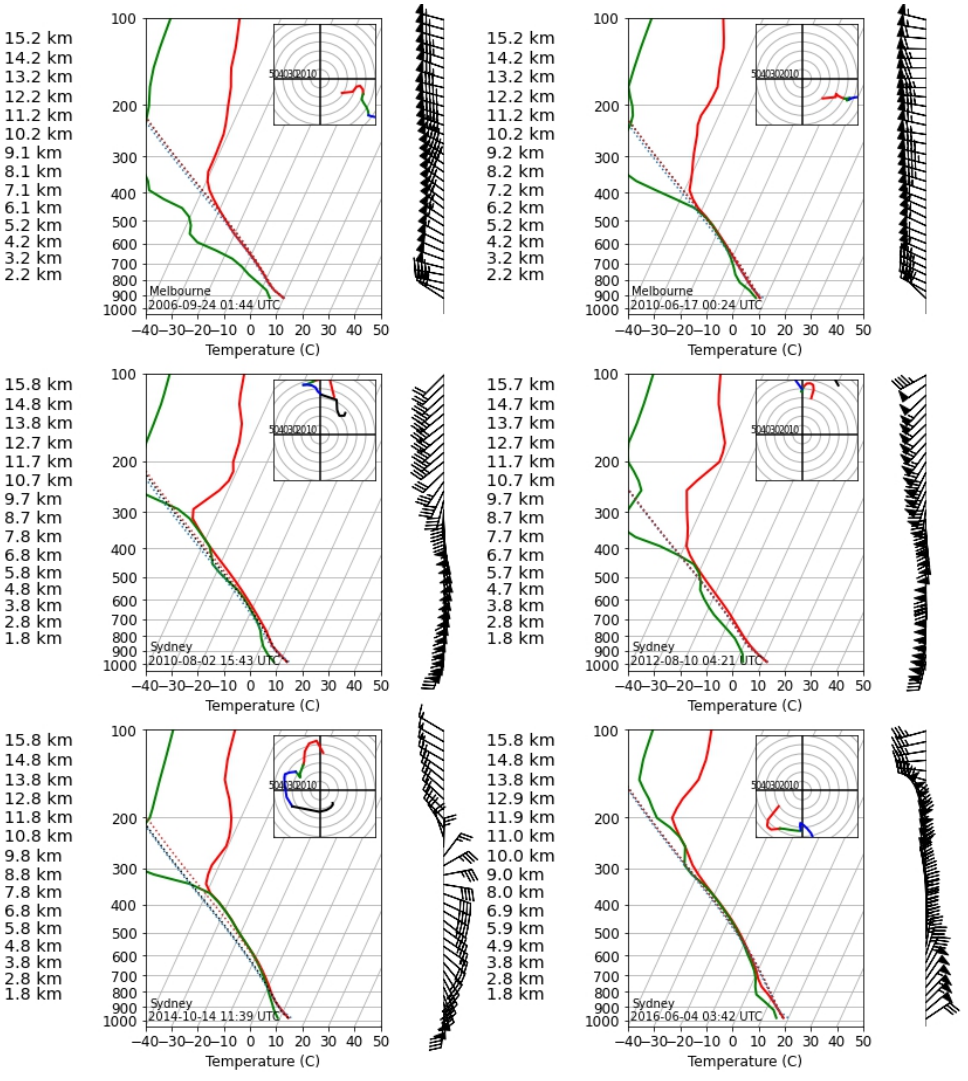

830 FIG. C1. As in Figure 13, but for each individual event within environmental cluster 1 (see Section 3d for
831 cluster definitions).

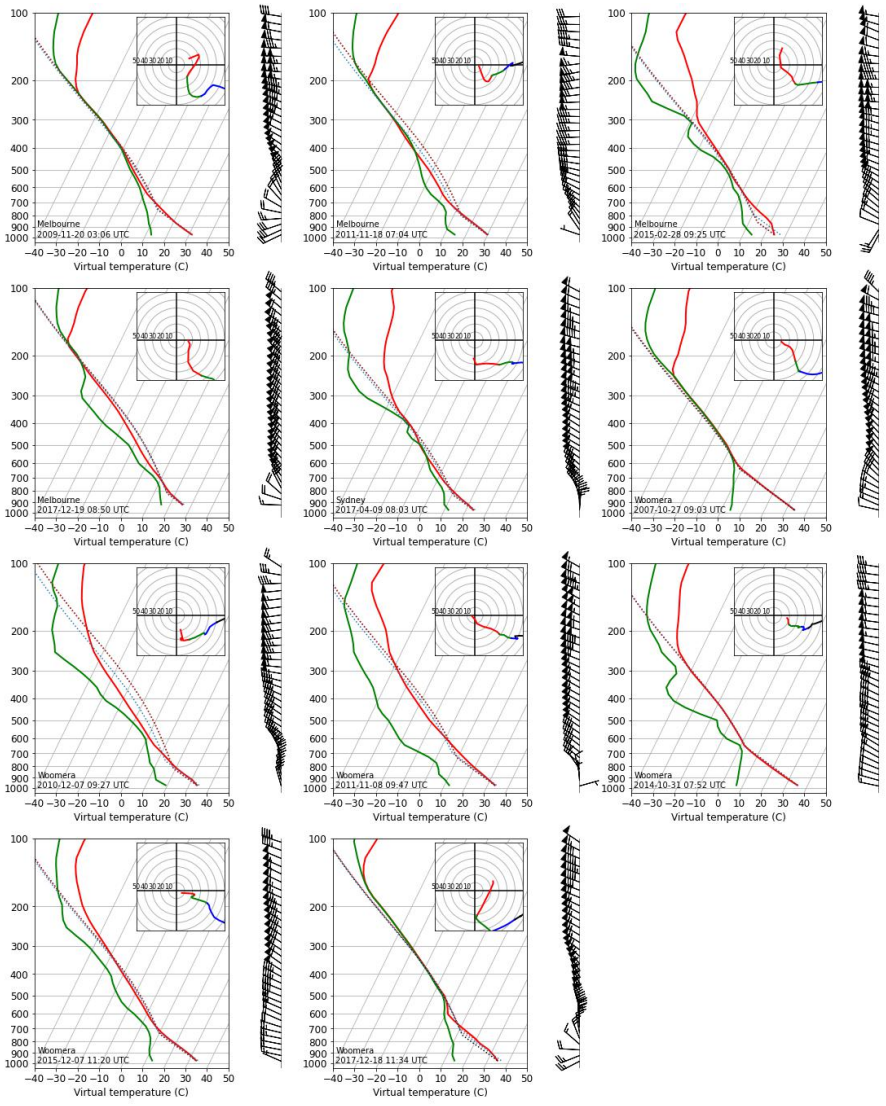

832 FIG. C2. As in Figure 13, but for each individual event within environmental cluster 2 (see Section 3d for
833 cluster definitions).

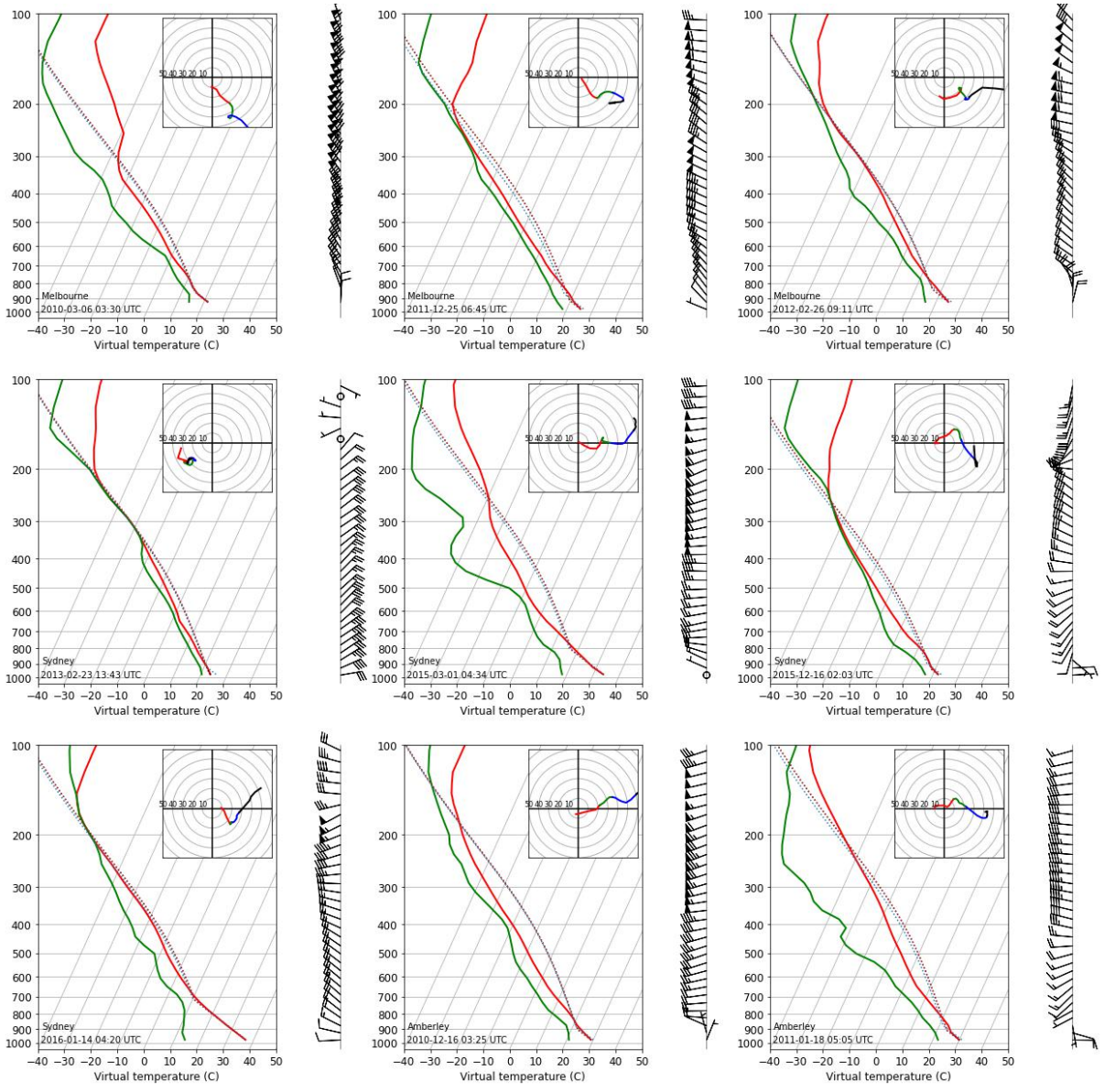

834 FIG. C3. As in Figure 13, but for nine individual events within environmental cluster 3 (see Section 3d for
835 cluster definitions). Continued in Figure C4 for the remaining 10 events in cluster 3.

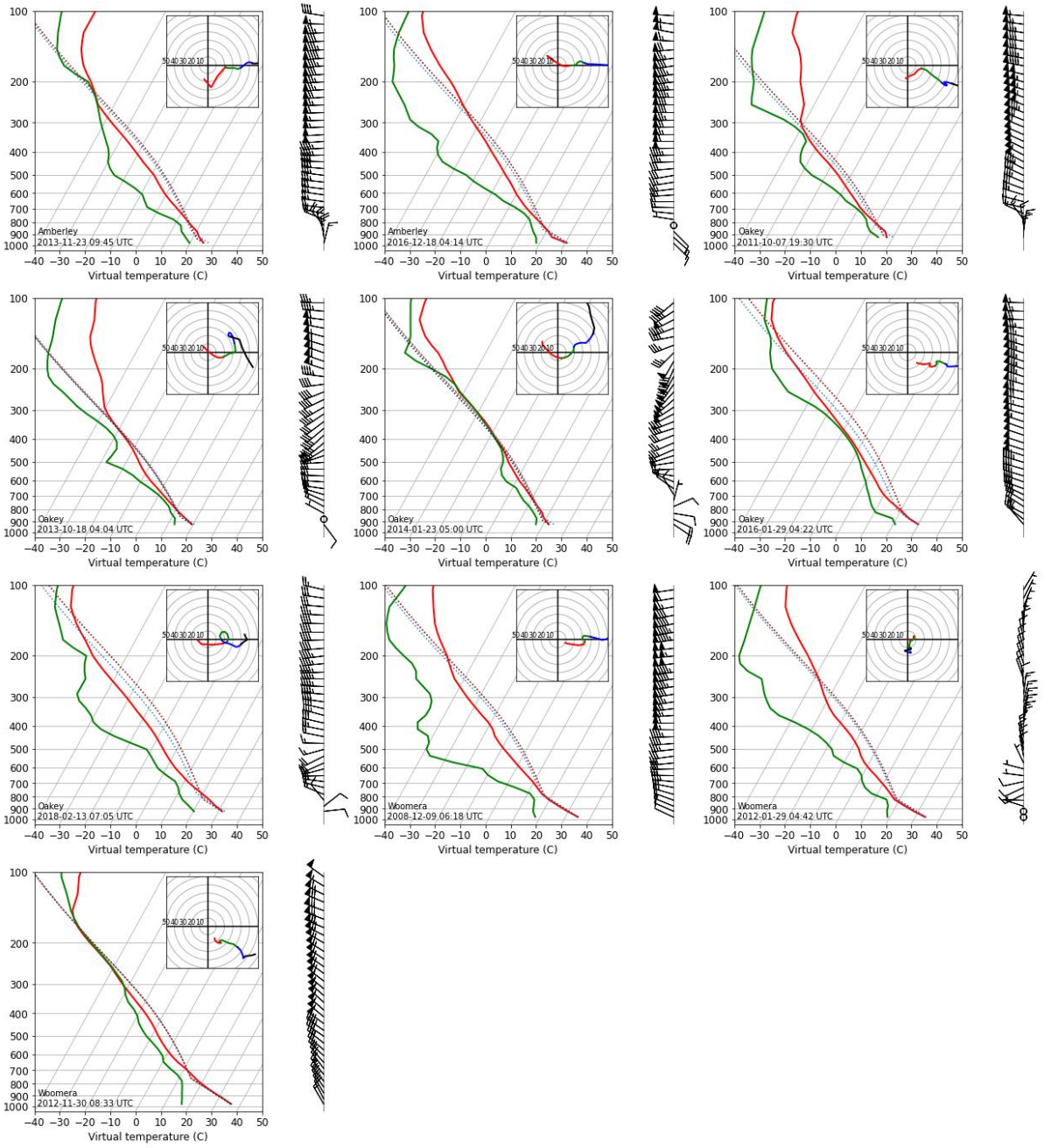

836 FIG. C4. As in Figure 13, but for ten individual events within environmental cluster 3 (see Section 3d for
837 cluster definitions).

References

Allen, J., 2012: Supercell Storms: Melbourne's white Christmas 2011. *Bulletin of the Australian Meteorological and Oceangraphic Society*, **25**, 47–51.

Atkins, N. T., and R. M. Wakimoto, 1991: Wet Microburst Activity over the Southeastern United States: Implications for Forecasting. *Weather and Forecasting*, **6 (4)**, 470–482, https://doi.org/10.1175/1520-0434(1991)006<0470:WMAOTS>2.0.CO;2, URL http://journals.ametsoc.org/doi/10.1175/1520-0434(1991)006%3C0470:WMAOTS%3E2.0.CO;2.

Blumberg, W. G., K. T. Halbert, T. A. Supinie, P. T. Marsh, R. L. Thompson, and J. A. Hart, 2017: Sharppy: An open-source sounding analysis toolkit for the atmospheric sciences. *Bulletin of the American Meteorological Society*, **98 (8)**, 1625–1636, https://doi.org/10.1175/BAMS-D-15-00309.1.

Brooks, H. E., 2013: Severe thunderstorms and climate change. *Atmospheric Research*, **123**, 129–138, https://doi.org/10.1016/j.atmosres.2012.04.002, URL http://dx.doi.org/10.1016/j.atmosres.2012.04.002.

Brown, A., and A. Dowdy, 2019: Extreme wind gusts and thunderstorms in South Australia analysed from 1979-2017 - Bureau Research Report 034. Tech. Rep. August, Australian Bureau of Meteorology, Melbourne, Australia.

Brown, A., and A. Dowdy, 2021a: Severe convection-related winds in Australia and their associated environments. *Journal of Southern Hemisphere Earth System Science*, https://doi.org/10.1071/ES19052, URL https://doi.org/10.1071/ES19052.

Brown, A., and A. Dowdy, 2021b: Severe Convective Wind Environments and Future Projected Changes in Australia. *Journal of Geophysical Research: Atmospheres*, **126 (16)**, 1–17, https://doi.org/10.1029/2021JD034633, URL https://onlinelibrary.wiley.com/doi/10.1029/2021JD034633.

Cintineo, J. L., M. J. Pavolonis, J. M. Sieglaff, L. Cronce, and J. Brunner, 2020: Noaa probsevere v2.0—probhail, probwind, and probtor. *Weather and Forecasting*, **35 (4)**, 1523–1543, https://doi.org/10.1175/WAF-D-19-0242.1.

Clark, M. R., 2013: A provisional climatology of cool-season convective lines in the UK. *Atmospheric Research*, **123**, 180–196, https://doi.org/10.1016/j.atmosres.2012.09.018, URL http://dx.doi.org/10.1016/j.atmosres.2012.09.018.

Corfidi, S., 2017: *Forecasting Severe Convective Storms*. April, https://doi.org/10.1093/acrefore/9780190228620.013.59.

CSIRO and Bureau of Meteorology, 2015: *Climate Change in Australia Information for Australia's National Resource Management Regions: Technical Report*. CSIRO and Bureau of Meteorology, Australia.

De Gaetano, P., M. P. Repetto, T. Repetto, and G. Solari, 2014: Separation and classification of extreme wind events from anemometric records. *Journal of Wind Engineering and Industrial Aerodynamics*, **126**, 132–143, https://doi.org/10.1016/j.jweia.2014.01.006, URL http://dx.doi.org/10.1016/j.jweia.2014.01.006.

Dowdy, A. J., and J. L. Catto, 2017: Extreme weather caused by concurrent cyclone , front and thunderstorm occurrences. *Nature Publishing Group*, 1–8, https://doi.org/10.1038/srep40359, URL http://dx.doi.org/10.1038/srep40359.

Dowdy, A. J., and Coauthors, 2019: Review of Australian east coast low pressure systems and associated extremes. *Climate Dynamics*, **53 (7)**, 4887–4910, https://doi.org/10.1007/s00382-019-04836-8, URL https://doi.org/10.1007/s00382-019-04836-8.

Durañona, V., M. Sterling, and C. J. Baker, 2007: An analysis of extreme non-synoptic winds. *Journal of Wind Engineering and Industrial Aerodynamics*, **95 (9-11)**, 1007–1027, https://doi.org/10.1016/j.jweia.2007.01.014.

Earl, N., S. Dorling, M. Starks, and R. Finch, 2017: Subsynoptic-scale features associated with extreme surface gusts in UK extratropical cyclone events. *Geophysical Research Letters*, **44 (8)**, 3932–3940, https://doi.org/10.1002/2017GL073124.

Earl, N., and I. Simmonds, 2018: Sub synoptic-scale features associated with extreme surface gusts during the South Australia Storm of September 2016 - Part II: analysis of mechanisms driving the gusts. *Weather*, https://doi.org/10.1002/wea.3384, URL http://doi.wiley.com/10.1002/wea.3384.

Gallus, W. A., N. A. Snook, and E. V. Johnson, 2008: Spring and summer severe weather reports over the midwest as a function of convective mode: A preliminary study. *Weather and Forecasting*, **23 (1)**, 101–113, https://doi.org/10.1175/2007WAF2006120.1.

Gatzen, C., 2013: Warm-season severe wind events in Germany. *Atmospheric Research*, **123**, 197–205, https://doi.org/10.1016/j.atmosres.2012.07.017, URL http://dx.doi.org/10.1016/j.atmosres.2012.07.017.

Geerts, B., 2001: Estimating Downburst-Related Maximum Surface Wind Speeds by Means of Proximity Soundings in New South Wales, Australia. *Weather and Forecasting*, **16 (2)**, 261–269, https://doi.org/10.1175/1520-0434(2001)016<0261:EDRMSW>2.0.CO;2, URL http://journals.ametsoc.org/doi/abs/10.1175/1520-0434%282001%29016%3C0261%3AEDRMSW%3E2.0.CO%3B2.

Heikenfeld, M., P. J. Marinescu, M. Christensen, D. Watson-Parris, F. Senf, S. C. van den Heever, and P. Stier, 2019: tobac 1.2: towards a flexible framework for tracking and analysis of clouds in diverse datasets. *Geoscientific Model Development*, **12 (11)**, 4551–4570, https://doi.org/10.5194/gmd-12-4551-2019, URL https://gmd.copernicus.org/articles/12/4551/2019/.

Helmus, J. J., and S. M. Collis, 2016: The Python ARM Radar Toolkit (Py-ART), a Library for Working with Weather Radar Data in the Python Programming Language. *Journal of Open Research Software*, **4**, https://doi.org/10.5334/jors.119.

Hersbach, H., and Coauthors, 2020: The ERA5 Global Reanalysis. *Quarterly Journal of the Royal Meteorological Society*, qj.3803, https://doi.org/10.1002/qj.3803, URL https://onlinelibrary.wiley.com/doi/abs/10.1002/qj.3803.

Hitchcock, S. M., T. P. Lane, R. A. Warren, and J. S. Soderholm, 2021: Linear rainfall features and their association with rainfall extremes near Melbourne, Australia. *Monthly Weather Review*, https://doi.org/10.1175/mwr-d-21-0007.1.

Holmes, J. D., 2002: A Re-analysis of Recorded Extreme Wind Speeds in Region A. *Australian Journal of Structural Engineering*, **4 (1)**, 29–40, https://doi.org/10.1080/13287982.2002.11464905, URL https://www.tandfonline.com/action/journalInformation?journalCode=tsen20.

Holmes, J. D., C.-H. Wang, and S. Oliver, 2018: Extreme winds for six South Australian locations. *Nineteenth Australasian Wind Engineering Society Workshop, April 4-6, 2018, Torquay, Victoria*, 1–6.

Holzworth, R. H., J. B. Brundell, M. P. McCarthy, A. R. Jacobson, C. J. Rodger, and T. S. Anderson, 2021: Lightning in the Arctic. *Geophysical Research Letters*, 1–6, https://doi.org/10.1029/2020gl091366.

Jacobson, A. R., R. Holzworth, J. Harlin, R. Dowden, and E. Lay, 2006: Performance assessment of the World Wide Lightning Location Network (WWLLN), using the Los Alamos Sferic Array (LASA) as ground truth. *Journal of Atmospheric and Oceanic Technology*, **23 (8)**, 1082–1092, https://doi.org/10.1175/JTECH1902.1.

Johns, R. H., and W. D. Hirt, 1987: Derechos: Widespread Convectively Induced Windstorms. *Weather and Forecasting*, **2 (1)**, 32–49, https://doi.org/10.1175/1520-0434(1987)002<0032:dwciw>2.0.co;2.

Klimowski, B. A., M. J. Bunkers, M. R. Hjelmfelt, and J. N. Covert, 2003: Severe convective windstorms over the northern High Plains of the United States. *Weather and Forecasting*, **18 (3)**, 502–519, https://doi.org/10.1175/1520-0434(2003)18<502:SCWOTN>2.0.CO;2.

Kuchera, E. L., and M. D. Parker, 2006: Severe Convective Wind Environments. *Weather and Forecasting*, **21 (4)**, 595–612, https://doi.org/10.1175/waf931.1.

Lagerquist, R., A. McGovern, and T. Smith, 2017: Machine Learning for Real-Time Prediction of Damaging Straight-Line Convective Wind. *Weather and Forecasting*, **32 (6)**, 2175–2193, https://doi.org/10.1175/WAF-D-17-0038.1, URL https://journals.ametsoc.org/doi/10.1175/WAF-D-17-0038.1.

Ludwig, P., J. G. Pinto, S. A. Hoepp, A. H. Fink, and S. L. Gray, 2015: Secondary cyclogenesis along an occluded front leading to damaging wind gusts: Windstorm Kyrill, January 2007. *Monthly Weather Review*, **143 (4)**, 1417–1437, https://doi.org/10.1175/MWR-D-14-00304.1.

Mahoney, K. M., G. M. Lackmann, and M. D. Parker, 2009: The role of momentum transport in the motion of a quasi-idealized mesoscale convective scale. *Monthly Weather Review*, **137 (10)**, 3316–3338, https://doi.org/10.1175/2009MWR2895.1.

Markowski, P. M., 2002: Hook echoes and rear-flank downdrafts: A review. *Monthly Weather Review*, **130 (4)**, 852–876, https://doi.org/10.1175/1520-0493(2002)130<0852:HEARFD>2.0.CO;2.

May, P. T., and A. Ballinger, 2007: The statistical characteristics of convective cells in a monsoon regime (Darwin, Northern Australia). *Monthly Weather Review*, **135 (1)**, 82–92, https://doi.org/10.1175/MWR3273.1.

Miller, M. L., V. Lakshmanan, and T. M. Smith, 2013: An automated method for depicting mesocyclone paths and intensities. *Weather and Forecasting*, **28 (3)**, 570–585, https://doi.org/10.1175/WAF-D-12-00065.1.

Miller, P. W., and T. L. Mote, 2018: Characterizing severe weather potential in synoptically weakly forced thunderstorm environments. *Natural Hazards and Earth System Sciences*, **18 (4)**, 1261–1277, https://doi.org/10.5194/nhess-18-1261-2018.

Mohr, S., M. Kunz, A. Richter, and B. Ruck, 2017: Statistical characteristics of convective wind gusts in Germany. *Natural Hazards and Earth System Sciences*, **17 (6)**, 957–969, https://doi.org/10.5194/nhess-17-957-2017.

Oliver, S. E., W. W. Moriarty, and J. D. Holmes, 2000: A risk model for design of transmission line systems against thunderstorm downburst winds. *Engineering Structures*, **22 (9)**, 1173–1179, https://doi.org/10.1016/S0141-0296(99)00057-7.

Pacey, G. P., D. M. Schultz, and L. Garcia-Carreras, 2021: Severe Convective Windstorms in Europe: Climatology, Preconvective Environments, and Convective Mode. *Weather and Forecasting*, **36 (1)**, 237–252, https://doi.org/10.1175/WAF-D-20-0075.1, URL https://journals.ametsoc.org/view/journals/wefo/36/1/WAF-D-20-0075.1.xml.

Pantillon, F., B. Adler, U. Corsmeier, P. Knippertz, A. Wieser, and A. Hansen, 2020: Formation of Wind Gusts in an Extratropical Cyclone in Light of Doppler Lidar Observations and Large-Eddy Simulations. *Monthly Weather Review*, **148 (1)**, 353–375, https://doi.org/10.1175/MWR-D-19-0241.1, URL http://journals.ametsoc.org/doi/10.1175/MWR-D-19-0241.1.

Pepler, A. S., A. J. Dowdy, and P. Hope, 2021: The differing role of weather systems in southern Australian rainfall between 1979–1996 and 1997–2015. *Climate Dynamics*, **56 (7-**

975 **8)**, 2289–2302, https://doi.org/10.1007/s00382-020-05588-6, URL https://doi.org/10.1007/
976 s00382-020-05588-6.

977 Potter, B. E., and J. R. Hernandez, 2017: Downdraft outflows: climatological potential to influence
978 fire behaviour. *International Journal of Wildland Fire*, **26 (8)**, 685, https://doi.org/10.1071/
979 wf17035.

980 Potts, R., 2002: Low altitude wind shear at major Australian airports and the risks to aviation.
981 *Preprints 10th Conf. on Aviation Range and Aerospace Meteorology, Amer. Met. Soc.*, Portland,
982 Oregon.

983 Potts, R., T. D. Keenan, and P. T. May, 2000: Radar characteristics of storms in the Sydney
984 area. *Monthly Weather Review*, **128 (9)**, 3308–3319, https://doi.org/10.1175/1520-0493(2000)
985 128<3308:RCOSIT>2.0.CO;2.

986 Prein, A. F., 2015: A review on regional convection-permitting climate modeling: Demonstrations,
987 prospects, and challenges. *Reviews of Geophysics*, **53 (2)**, 323–361, https://doi.org/10.1002/
988 2014rg000475.

989 Proctor, F. H., 1989: Numerical simulations of an isolated microburst. Part II: sensitivity experi-
990 ments. 2143–2165 pp., https://doi.org/10.1175/1520-0469(1989)046<2143:NSOAIM>2.0.CO;
991 2.

992 Pryor, K. L., 2015: Progress and developments of downburst prediction applications of GOES.
993 *Weather and Forecasting*, **30 (5)**, 1182–1200, https://doi.org/10.1175/WAF-D-14-00106.1.

994 Raut, B. A., R. Jackson, M. Picel, S. M. Collis, M. Bergemann, and C. Jakob, 2021: An adaptive
995 tracking algorithm for convection in simulated and remote sensing data. *Journal of Applied*
996 *Meteorology and Climatology*, **60 (4)**, 513–526, https://doi.org/10.1175/JAMC-D-20-0119.1.

997 Richter, H., 2007: A cool season low-topped supercell tornado event near Sydney, Australia. *33rd*
998 *International Conference on Radar Meteorology, Cairns, Australia, 6-10 August 2007*, 110.

999 Richter, H., J. Peter, and S. Collis, 2014: Analysis of a Destructive Wind Storm on 16 November
1000 2008 in Brisbane, Australia. *Monthly Weather Review*, **142 (9)**, 3038–3060, https://doi.org/
1001 10.1175/mwr-d-13-00405.1.

Schumacher, R. S., and K. L. Rasmussen, 2020: The formation, character and changing nature of mesoscale convective systems. *Nature Reviews Earth & Environment*, **1 (6)**, 300–314, https://doi.org/10.1038/s43017-020-0057-7, URL http://dx.doi.org/10.1038/s43017-020-0057-7.

Seneviratne, S., and Coauthors, 2021: *Weather and Climate Extreme Events in a Changing Climate. In Climate Change 2021: The Physical Science Basis. Contribution of Working Group I to the Sixth Assessment Report of the Intergovernmental Panel on Climate Change*. Cambridge University Press. In Press.

Sherburn, K. D., M. J. Bunkers, and A. J. Mose, 2021: Radar-Based Comparison of Thunderstorm Outflow Boundary Speeds versus Peak Wind Gusts from Automated Stations. *Weather and Forecasting*, 1–50, https://doi.org/10.1175/waf-d-20-0221.1.

Sherman, D. J., 1987: The Passage of a Weak Thunderstorn Downburst over an Instrumented Tower. *Monthly Weather Review*, **115 (6)**, 1193–1205, URL https://doi.org/10.1175/1520-0493(1987)115%3C1193:TPOAWT%3E2.0.CO;2.

Smith, B. T., T. E. Castellanos, A. C. Winters, C. M. Mead, A. R. Dean, and R. L. Thompson, 2013: Measured Severe Convective Wind Climatology and Associated Convective Modes of Thunderstorms in the Contiguous United States, 2003–09. *Weather and Forecasting*, **28 (1)**, 229–236, https://doi.org/10.1175/WAF-D-12-00096.1, URL https://journals.ametsoc.org/doi/10.1175/WAF-D-12-00096.1.

Smith, B. T., R. L. Thompson, J. S. Grams, C. Broyles, and H. E. Brooks, 2012: Convective modes for significant severe thunderstorms in the contiguous United States. Part I: Storm classification and climatology. *Weather and Forecasting*, **27 (5)**, 1114–1135, https://doi.org/10.1175/WAF-D-11-00115.1.

Sobash, R. A., J. S. Kain, D. R. Bright, A. R. Dean, M. C. Coniglio, and S. J. Weiss, 2011: Probabilistic forecast guidance for severe thunderstorms based on the identification of extreme phenomena in convection-allowing model forecasts. *Weather and Forecasting*, **26 (5)**, 714–728, https://doi.org/10.1175/WAF-D-10-05046.1.

Soderholm, J. S., H. McGowan, H. Richter, K. Walsh, T. M. Weckwerth, and M. Coleman, 2017: An 18-year climatology of hailstorm trends and related drivers across southeast Queensland, Australia. *Quarterly Journal of the Royal Meteorological Society*, **143 (703)**, 1123–1135, https://doi.org/10.1002/qj.2995.

Soderholm, J. S., A. Protat, and C. Jakob, 2019: Australian Operational Weather Radar Dataset. National Computing Infrastructure, https://doi.org/10.25914/5cb686a8d9450.

Spassiani, A. C., and M. S. Mason, 2021: Application of Self-organizing Maps to classify the meteorological origin of wind gusts in Australia. *Journal of Wind Engineering and Industrial Aerodynamics*, **210 (January)**, 104 529, https://doi.org/10.1016/j.jweia.2021.104529, URL https://doi.org/10.1016/j.jweia.2021.104529.

Srivastava, R. C., 1985: A simple model of evaporatively driven downdraft: Application to microburst downdraft. *Journal of the Atmospheric Sciences*, **42 (10)**, 1004–1023.

Steiner, M., R. A. Houze, and S. E. Yuter, 1995: Climatological Characterization of Three-Dimensional Storm Structure from Operational Radar and Rain Gauge Data. *Journal of Applied Meteorology*, **34 (9)**, 1978–2007, https://doi.org/10.1175/1520-0450(1995)034<1978:CCOTDS>2.0.CO;2, URL http://journals.ametsoc.org/doi/10.1175/1520-0450(1995)034%3C1978:CCOTDS%3E2.0.CO;2.

Su, C.-H., and Coauthors, 2018: BARRA v1.0: The Bureau of Meteorology Atmospheric high-resolution Regional Reanalysis for Australia. *Geoscientific Model Development Discussions*, **(December)**, 1–33, https://doi.org/10.5194/gmd-2018-277.

Taszarek, M., J. T. Allen, P. Groenemeijer, R. Edwards, H. E. Brooks, V. Chmielewski, and S.-E. Enno, 2020a: Severe convective storms across Europe and the United States. Part 1: Climatology of lightning, large hail, severe wind and tornadoes. *Journal of Climate*, 1–47, https://doi.org/10.1175/JCLI-D-20-0345.1, URL https://journals.ametsoc.org/jcli/article/354771/Severe-convective-storms-across-Europe-and-the.

Taszarek, M., J. T. Allen, T. Púčik, K. A. Hoogewind, and H. E. Brooks, 2020b: Severe convective storms across Europe and the United States. Part 2: ERA5 environments

associated with lightning, large hail, severe wind and tornadoes. *Journal of Climate*, 1–53, https://doi.org/10.1175/JCLI-D-20-0346.1, URL https://journals.ametsoc.org/jcli/article/354770/Severe-convective-storms-across-Europe-and-the.

Taszarek, M., H. E. Brooks, and B. Czernecki, 2017: Sounding-Derived Parameters Associated with Convective Hazards in Europe. *Monthly Weather Review*, **145 (4)**, 1511–1528, https://doi.org/10.1175/MWR-D-16-0384.1, URL http://journals.ametsoc.org/doi/10.1175/MWR-D-16-0384.1.

Thompson, R. L., R. Edwards, and C. M. Mead, 2004: An update to the Supercell Composite and Significant Tornado Parameters. Tech. rep., Storm Prediction Center, Norman, OK.

Thompson, R. L., C. M. Mead, and R. Edwards, 2007: Effective storm-relative helicity and bulk shear in supercell thunderstorm environments. *Weather and Forecasting*, **22 (1)**, 102–115, https://doi.org/10.1175/WAF969.1.

Thompson, R. L., B. T. Smith, J. S. Grams, A. R. Dean, and C. Broyles, 2012: Convective modes for significant severe thunderstorms in the contiguous United States. Part II: Supercell and QLCS tornado environments. *Weather and Forecasting*, **27 (5)**, 1136–1154, https://doi.org/10.1175/WAF-D-11-00116.1.

van den Broeke, M. S., D. M. Schultz, R. H. Johns, J. S. Evans, and J. E. Hales, 2005: Cloud-to-ground lightning production in strongly forced, low-instability, convective lines associated with damaging wind. *Weather and Forecasting*, **20 (4)**, 517–530, https://doi.org/10.1175/WAF876.1.

Virts, K. S., J. M. Wallace, M. L. Hutchins, and R. H. Holzworth, 2013: Highlights of a new ground-based, hourly global lightning climatology. *Bulletin of the American Meteorological Society*, **94 (9)**, 1381–1391, https://doi.org/10.1175/BAMS-D-12-00082.1.

Wakimoto, R. M., 1985: Forecasting dry microburst activity over the High Plains. *Monthly Weather Review*, **113**, 1131–1143.

Wakimoto, R. M., 2001: Convectively Driven High Wind Events. *Severe Convective Storms*, C. A. Doswell, Ed., American Meteorological Society, Boston, MA, 255–298, https://doi.org/10.1007/978-1-935704-06-5{_}7, URL https://doi.org/10.1007/978-1-935704-06-5_7.

Wakimoto, R. M., H. V. Murphey, C. A. Davis, and N. T. Atkins, 2006: High winds generated by bow echoes. Part II: The relationship between the mesovortices and damaging straight-line winds. *Monthly Weather Review*, **134 (10)**, 2813–2829, https://doi.org/10.1175/MWR3216.1.

Warren, R. A., C. Jakob, S. M. Hitchcock, and B. A. White, 2021: Heavy versus extreme rainfall events in southeast Australia. *Quarterly Journal of the Royal Meteorological Society*, **147 (739)**, 3201–3226, https://doi.org/10.1002/qj.4124, URL https://onlinelibrary.wiley.com/doi/10.1002/qj.4124.

Warren, R. A., H. A. Ramsay, S. T. Siems, M. J. Manton, J. R. Peter, A. Protat, and A. Pillalamarri, 2020: Radar-based climatology of damaging hailstorms in Brisbane and Sydney, Australia. *Quarterly Journal of the Royal Meteorological Society*, **146 (726)**, 505–530, https://doi.org/10.1002/qj.3693.

Weisman, M. L., 1992: The role of convectively generated rear-inflow jets in the evolution of long-lived mesoconvective systems. 1826–1847 pp., https://doi.org/10.1175/1520-0469(1992)049<1826:TROCGR>2.0.CO;2.

Weisman, M. L., and J. B. Klemp, 1982: The Dependence of Numerically Simulated Convective Storms on Vertical Wind Shear and Buoyancy. *Monthly Weather Review*, **110 (6)**, 504–520, https://doi.org/https://doi.org/10.1175/1520-0493(1982)110<0504:TDONSC>2.0.CO;2.

Weisman, M. L., and R. Rotunno, 2004: "A theory for strong long-lived squall lines" revisited. *Journal of the Atmospheric Sciences*, **61 (4)**, 361–382, https://doi.org/10.1175/1520-0469(2004)061<0361:ATFSLS>2.0.CO;2.

Weisman, M. L., and R. J. Trapp, 2003: Low-level mesovortices within squall lines and bow echoes. Part I: Overview and dependence on environmental shear. *Monthly Weather Review*, **131 (11)**, 2779–2803, https://doi.org/10.1175/1520-0493(2003)131<2779:LMWSLA>2.0.CO;2.

Yang, X., and J. Sun, 2018: Organizational Modes of Severe Wind-producing Convective Systems over North China. *Advances in Atmospheric Sciences*, **35 (5)**, 540–549, https://doi.org/10.1007/s00376-017-7114-2.

Yang, X., J. Sun, and Y. Zheng, 2017: A 5-yr Climatology of Severe Convective Wind Events over China. *Weather and Forecasting*, **32 (4)**, 1289–1299, https://doi.org/10.1175/waf-d-16-0101.1.

1111 Ye, B., A. D. Del Genio, and K. K. Lo, 1998: CAPE variations in the current climate and in a climate
1112 change. *Journal of Climate*, **11 (8)**, 1997–2015, https://doi.org/10.1175/1520-0442-11.8.1997.

1113 Zhou, Z., Q. Zhang, J. T. Allen, X. Ni, and C. Ng, 2021: How Many Types of Severe Hailstorm
1114 Environments Are There Globally? *Geophysical Research Letters*, **48 (23)**, 1–11, https://doi.org/
1115 10.1029/2021GL095485, URL https://onlinelibrary.wiley.com/doi/10.1029/2021GL095485.